NOISE CHARACTERISTICS OF TUNNEL DIODES

A Thesis

Presented to

the Faculty of Graduate Studies and Research

The University of Manitoba

In Partial Fulfillment

of the Requirements for the Degree

Master of Science in Electrical Engineering

---

by

Jacob Abraham Wiens

February 1963

ABSTRACT

The basic mechanism producing the well-known shot noise in a tunnel diode is outlined. Fluctuation noise, such as thermal noise, shot noise, flicker noise, excess noise, and contact noise as associated with resistors, diodes, and semiconductors, is briefly described. A review of the equivalent circuit and stability criterion of the tunnel diode is also included. Noise measurements of a germanium tunnel diode are performed at frequencies of 30 and 60 megacycles per second for the complete range of the forward bias region.

PREFACE

In October 1957 Leo Esaki, a Japanese physicist, announced the discovery of a narrow p-n junction characterized by a negative conductance region.[1]* He noted that the anomalous negative conductance was due to a tunneling current now called the Esaki current. Theoretical work dating back to 1929 has indicated the possibility of a phenomenon called the "tunneling effect". As early as 1954, P. Aigrain had indicated the possibility of tunneling occurring in high impurity p-n junctions.[2]

The generation of shot noise in tunnel diodes was first suggested by Chang and was further investigated by Tiemann.[3,4]

In the first chapter a brief introduction is given of the junction currents present in the tunnel diode and how they contribute to the generation of shot noise. The second chapter discusses the individual junction currents in a qualitative manner and the third chapter describes the magnitude of the shot noise contributed by each of the junction currents.

Since a reference noise is required to facilitate the noise measurements of the tunnel diode, all of the fourth chapter is devoted to a noise study in components such as vacuum diodes and resistors. The fifth chapter outlines briefly the effect of the parasitic resistance on the shot noise measurement of the tunnel diode. Due to the difficulty in stabilizing the tunnel diode in the negative con-

---

* The numberal denotes the reference number as listed in the bibliography.

ductance region for its noise measurements, the sixth chapter discusses the stability criterion with the aid of the Hurwitz criterion. In the seventh chapter the tests and measuring techniques for the tunnel diode noise measurement are outlined. The eighth and last chapter includes a discussion of the results and conclusions.

The appendix contains the test circuit for the measurement of the tunnel diode current-voltage characteristic. Also contained in the appendix are the noise figure measurements of the receiver systems which were used for the tunnel diode noise measurements. The specifications of the tunnel diode 1N2939 are also included in the appendix.

Finally, the author wishes to express his sincere thanks to Professor Ernest Bridges for his many helpful suggestions and the University of Manitoba for its financial assistance.

TABLE OF CONTENTS

APPENDICES PAGE

LIST OF FIGURES

CHAPTER I

INTRODUCTION

The tunnel diode, a single p-n junction, is characterized by a negative conductance region over a section of its forward characteristic. Figure 1.1 illustrates the negative conductance region lying between two positive conductance regions.

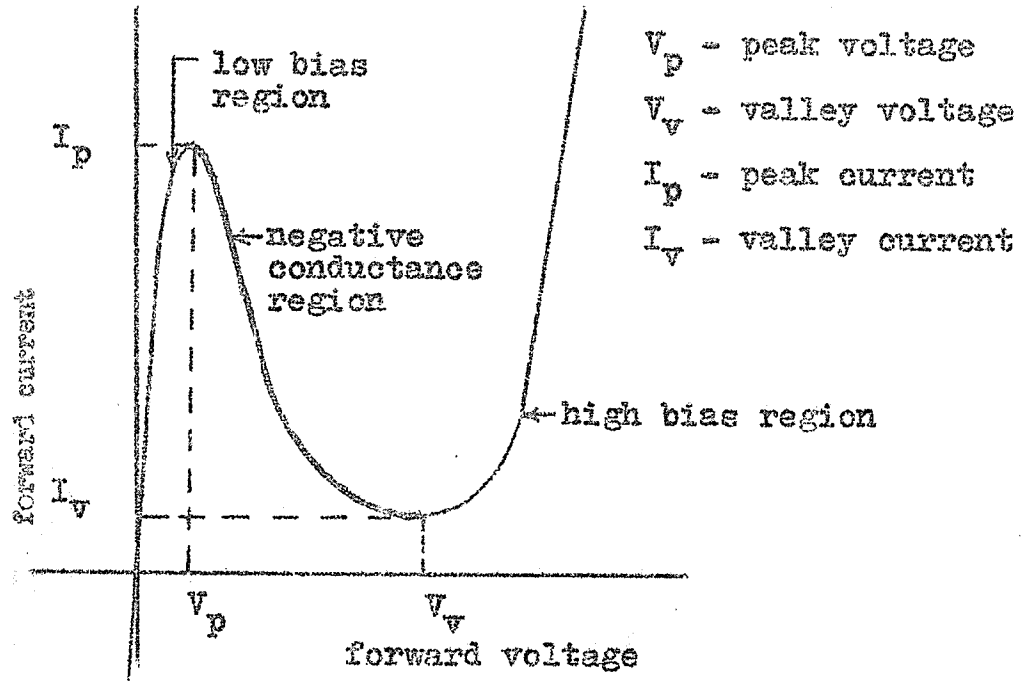

Figure 1.1 Typical tunnel diode characteristic curve.

The parameters V_p and V_v are dependent on the type of semiconductor used (germanium, silicon, or gallium arsenide). However, the peak current I_p is determined by the cross-sectional area of the junction and the amount of impurity present in the junction.

The resultant characteristic curve of figure 1.1 is composed of four individual currents as shown in figure 1.2[4]

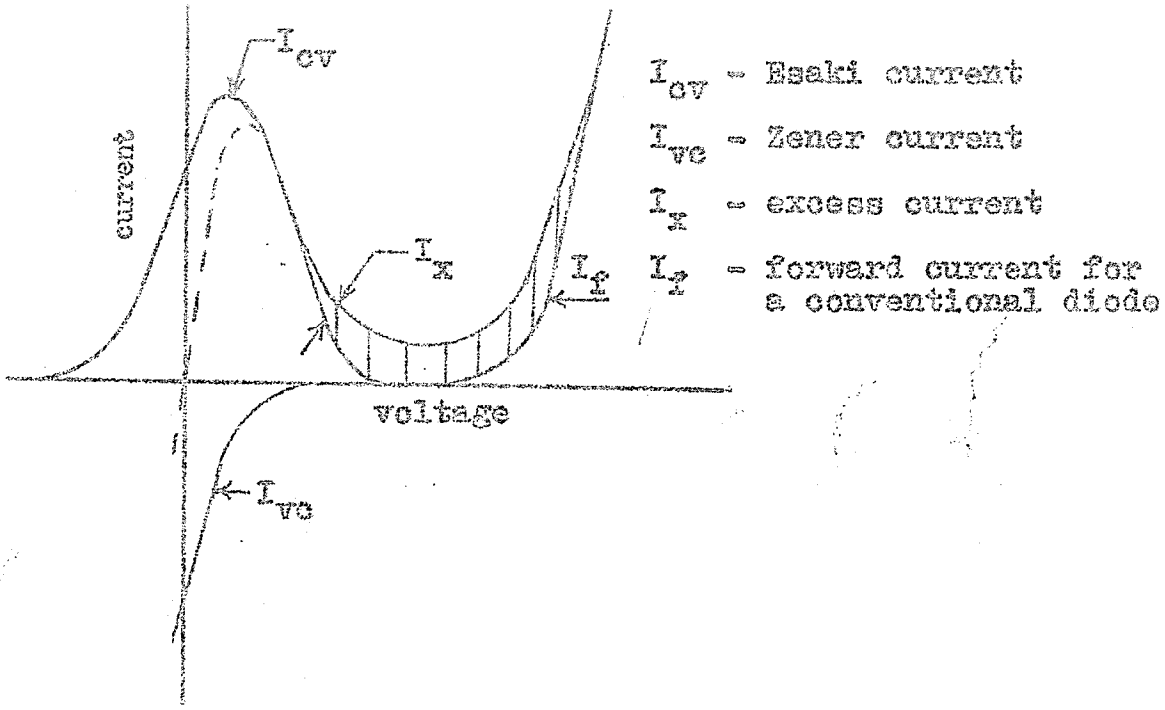

Figure 1.2 Internal junction currents of the tunnel diode.

The net characteristic current in the positive bias region may be expressed as

$$I_o = I_{ov} + I_{vc} + I_x + I_f \quad \text{..... 1.1}$$

The currents I_{ov}, I_{vc}, I_x, and I_f are known to be uncorrelated giving rise to an average equivalent shot noise current of

$$I_{eq} = I_{ov} + |I_{vc}| + I_x + I_f' \quad \text{..... 1.2}$$

where I_f' is the equivalent shot noise current for a conventional diode and is approximately equal to I_f for large forward voltages. Figure 1.3 shows the equivalent shot noise current in the positive bias region.

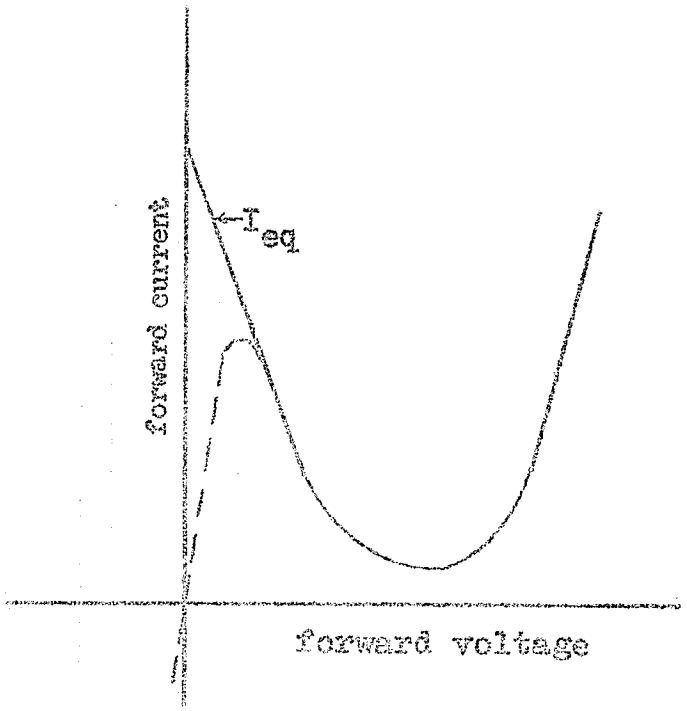

Figure 1.3 The equivalent shot noise current for a typical tunnel diode at room temperature.

The root mean square shot noise current may be expressed as[4]

$$\overline{i^2} = 2qI_{eq}B \quad \text{..... 1.3}$$

where q is the charge of an electron

(1.59×10^{-19} coulombs)

and B is the noise bandwidth of the measuring device in cycles per second.

CHAPTER II

QUALITATIVE DESCRIPTION OF THE TUNNEL DIODE

CURRENT CHARACTERISTICS

Only the Esaki and the Zener currents are known to exist in the low bias region. It is therefore possible to express the sum of the Esaki and Zener currents in terms of the resultant diode current. The mechanism leading to the excess current is at present not fully understood. However, a generally accepted explanation supported by experimental evidence is given.

I. ESAKI AND ZENER CURRENTS

The Esaki and Zener currents are produced by the quantum mechanical tunneling of electrons through the forbidden band of the junction region giving rise to a negative conductance of the tunnel diode. The two requirements which must be met for tunneling to occur are that the depletion region of the junction must be narrow and that the n-type and p-type semiconductors must be degenerate. An electron approaching the barrier has an infinitesimal probability of tunneling through the barrier to an unfilled state of equal energy on the opposite side of the barrier, even though the electron does not have the energy to surmount the potential hill. Tunneling may occur just as readily against an electric field as with it.

The energy band diagram of a tunnel diode p-n junction

is shown in figure 2.1[5,6,19]. The Fermi levels $E_{f(p)}$ and $E_{f(n)}$ for the p-type and n-type semiconductors respectively are brought into alignment at zero bias or at temperature equilibrium.

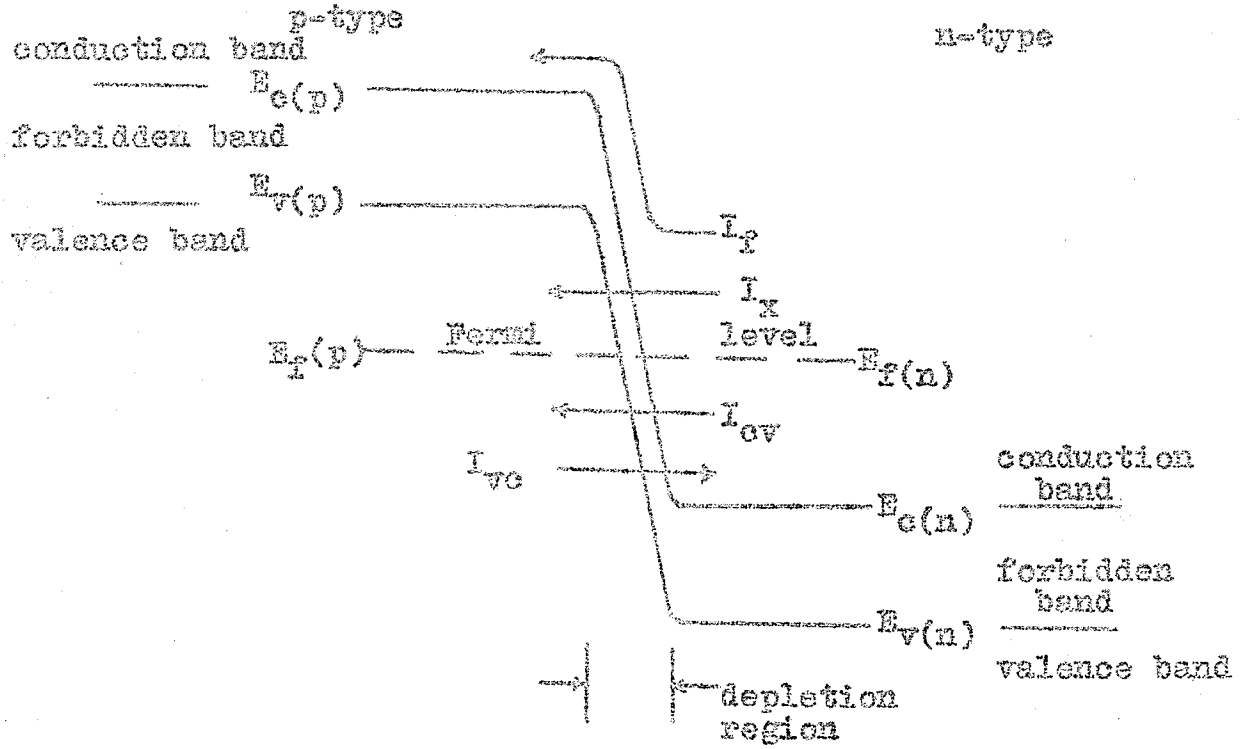

Figure 2.1 The tunnel diode energy band diagram for zero external bias.

E_c is the band edge representing the lowest energy level of the conduction band and E_v is the band edge representing the highest energy level of the valence band.

The expression for the Esaki and Zener currents as formulated by Esaki are respectively[1]

$$I_{cv} = A\int_{E_{c(n)}}^{E_{v(p)}} f_c \rho_c Z_{cv} (1-f_v)\rho_v dE \quad \ldots\ldots\ldots\ldots\ldots 2.1$$

and $$I_{vc} = A\int_{E_{c(n)}}^{E_{v(p)}} f_v \rho_v Z_{vc} (1-f_c)\rho_c dE \quad \ldots\ldots\ldots\ldots\ldots 2.2$$

where f_v and f_c are the Fermi-Dirac distribution functions for the valence and conduction band respectively; ρ_v and ρ_c are the energy level densities in the conduction and valence band respectively and are known to behave in a simple square law relationship equal to $\sqrt{E_{v(p)} - E}$ and $\sqrt{E - E_{c(n)}}$ respectively. Z_{cv} and Z_{vc} are the tunneling transition probabilities which can be assumed to be approximately equal, and A is a constant related to the junction area.

The expression for the Fermi-Dirac distribution function is given as[24]

$$f(E) = \frac{1}{\exp. \frac{E-E_f}{KT} + 1} \quad \text{..... 2.3}$$

where E is the energy level of the electron, E_f is the Fermi level, T is the temperature in degrees Kelvin and K is the Boltzmann constant.

Figure 2.2 shows, by means of a simple energy band scheme, the variables within the integral of the expressions 2.1 and 2.2.

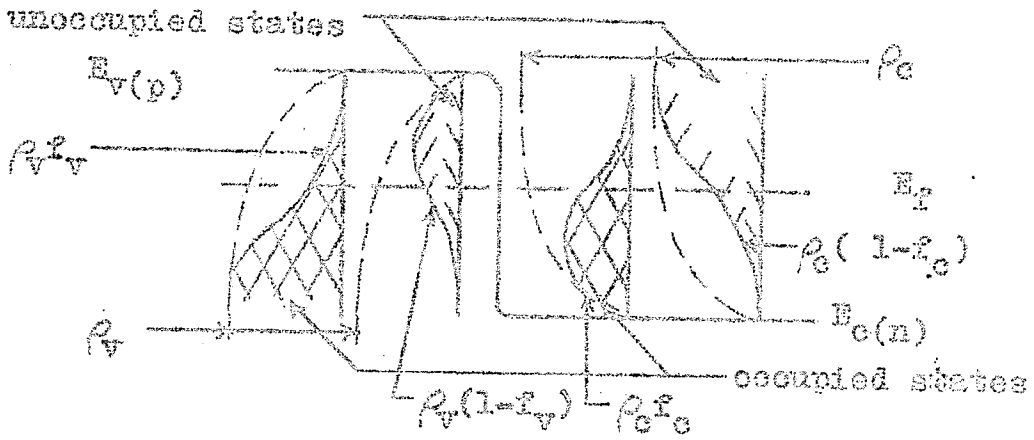

Figure 2.2 Energy band diagram showing the vacant and filled energy states.

A current increment of I_{cv} tunneling from the conduction band to the valence band is proportional to the number of electrons available in the conduction band $\rho_c f_c$, times the tunneling probability Z_{cv}, times the number of available or unoccupied states $\rho_v(1-f_v)$ in the valence band. Similarly, a current increment of I_{vc} tunnels from the valence band to the conduction band.

The resultant tunneling current in the forward direction through the barrier is[7]

$$I_{cv} - I_{vc} = A\int_{E_{c(n)}}^{E_{v(p)}} \left[f_c(E)-f_v(E)\right]\sqrt{E-E_{c(n)}}\sqrt{E_{v(p)}-E}\,dE \quad \ldots 2.4$$

where $f_c(E) - f_v(E)$ is represented graphically in figure 2.3 and the product of the energy level densities are represented in figure 2.4.

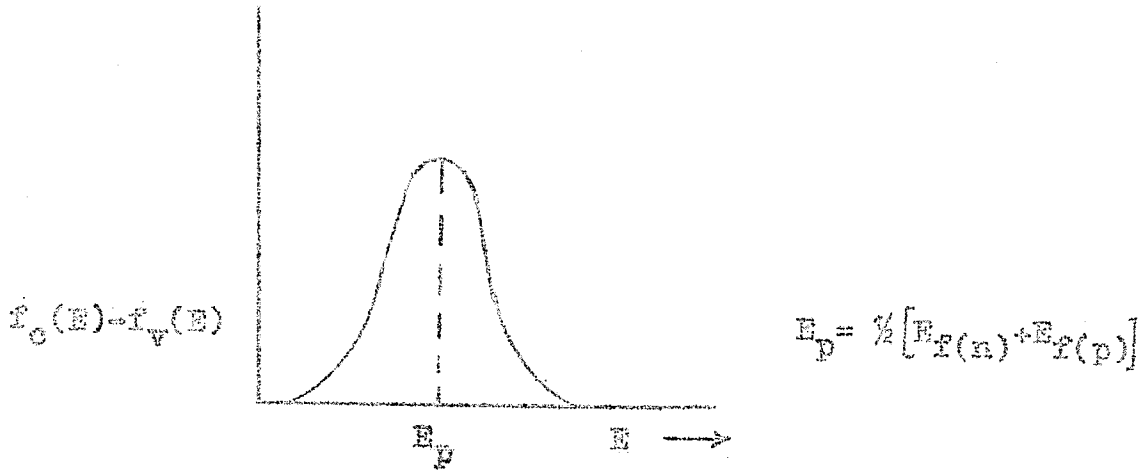

Figure 2.3 Graph of $f_c(E) - f_v(E)$ versus E.

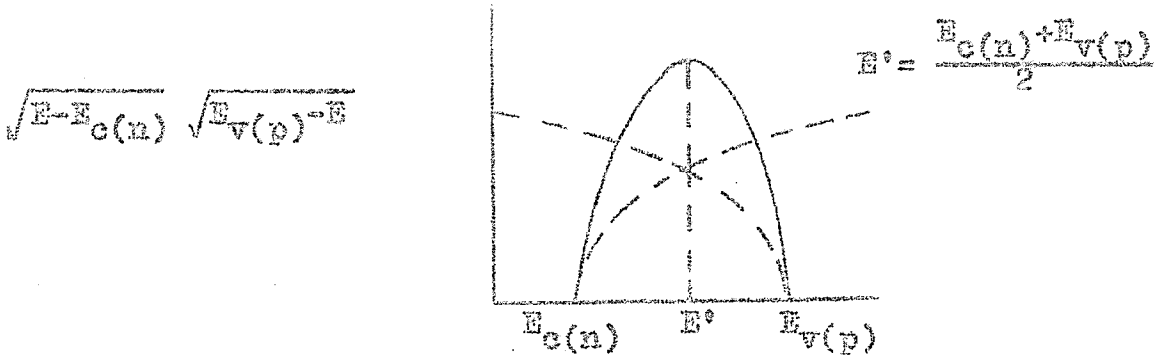

Figure 2.4 Graph of $\sqrt{E-E_{c(n)}}\ \sqrt{E_{v(p)}-E}$ versus E

The graphs of figures 2.3 and 2.4 may be superimposed for constant values of bias voltage. This is done for a number of voltage points ranging from zero to $(E_{f(n)}-E_{f(p)})/q$ resulting in the current voltage curve shown in figure 2.5. I'_c represents the corrected current-voltage characteristic due to the parasitic resistance. In other words the voltage drop across the bulk resistance R_s has been subtracted from the terminal voltage of the tunnel diode.

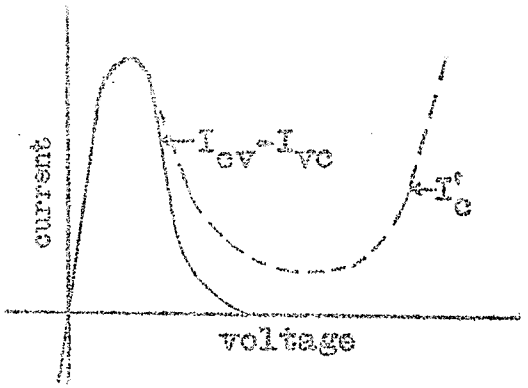

Figure 2.5 Resultant current-voltage curve due to the Zener and Esaki currents.

From figure 2.5 it can be seen that the sum of the Zener and Esaki current is equal to I_c' up to a bias voltage slightly exceeding the peak voltage. The Zener and Esaki currents can therefore be expressed in terms of I_c'. In order to perform the operation it is necessary to express $f_v(1-f_c)$ as a function of $f_c(1-f_v)$.[8] From figure 2.1 the Fermi levels $E_{f(p)}$ and $E_{f(n)}$ are related by the following expression when an external bias voltage V is applied.

$$E_{f(p)} = E_{f(n)} - qV \qquad \ldots\ldots 2.5$$

With the use of expressions 2.3 and 2.5 it is found that

$$f_v(1-f_c) = f_c(1-f_v)e^{\frac{-qV}{KT}} \qquad \ldots\ldots 2.6$$

By performing the proper substitutions into expressions 2.1 and 2.2 it follows that

$$I_{vc} = I_{cv}e^{\frac{-qV}{KT}} \qquad \ldots\ldots 2.7$$

For the low bias region

$$I_c' = I_{cv} - I_{vc} \qquad \ldots\ldots 2.8$$

The expression for I_{cv} and I_{vc} may now be solved by simple substitution to give

$$I_{cv} = \frac{I_c'}{1 - \exp.\frac{-qV}{KT}} \qquad \ldots\ldots 2.9$$

and

$$I_{vc} = \frac{I_c'}{\exp.\frac{qV}{KT} - 1} \qquad \ldots\ldots 2.10$$

Figure 2.8 shows the calculated values of I_{cv} and I_{vc} for the tunnel diode IN2939.

II. EXCESS CURRENT

The excess current occurs when the band edge $E_{c(n)}$ is raised to a higher level of energy than the band edge $E_{v(p)}$. According to the former tunneling theory of the Esaki and Zener currents as shown in figure 2.5, this current should not exist.

The mechanism which appears to be generally accepted is that in which the excess current is caused by electrons tunneling part of the way through the forbidden region. This mechanism was first suggested by Yakima and Esaki and has been confirmed by them by deliberately changing the imperfection of the junction by doping and by radiation damage.[9] The peak and excess current ratio was found to be insensitive to the doping concentrations thereby indicating that the mechanism of both currents is possibly the same.

Figure 2.6 shows several paths which the electrons may follow.

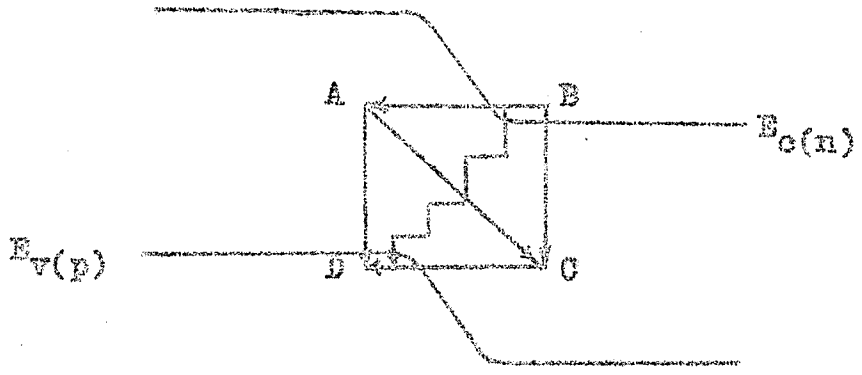

Figure 2.6 Possible paths for electron tunneling.

Four possible paths for electron travel are BAD, BCD, BACD or the staircase BD. The path BCD is considered to be the basic mechanism and the other paths, although more complicated, are unlikely to produce any radically different behaviour. If energy levels are considered to exist in the forbidden region in the n-type conductor, then the tunneling electrons are said to be replenished at point C.

Electron tunneling created by the presence of impurity levels existing in the energy gap is known as field ionization. The two types of energy states existing in the energy gap due to the heavy impurity concentrations are the deep level traps and those due to general fuzzing of the band edge. The deep level electron trap has the property of capturing an electron and holding it for an appreciable length of time before permitting it to leave. Similarly, hole traps will retain a hole for an appreciable length of time before the holes recombine. The excess current I_x for the tunnel diode 1N2939 is shown in figure 2.8.

III. CONVENTIONAL DIODE FORWARD CURRENT

At sufficiently large bias the current may be approximated by[1]

$$I_f = K\left(e^{\frac{qV}{KT}} - 1\right) \quad \text{..... 2.11}$$

This is the expression for the conventional forward minority carrier injection current. If the current voltage character-

istic curve is plotted on a semilogarithmic graph as shown in figure 2.7, the characteristic curve will gradually approach a line of slope $\frac{q}{KT}$ for an increase of the forward voltage. It may be necessary to exceed the maximum current limitation of the diode in order to arrive at this slope.

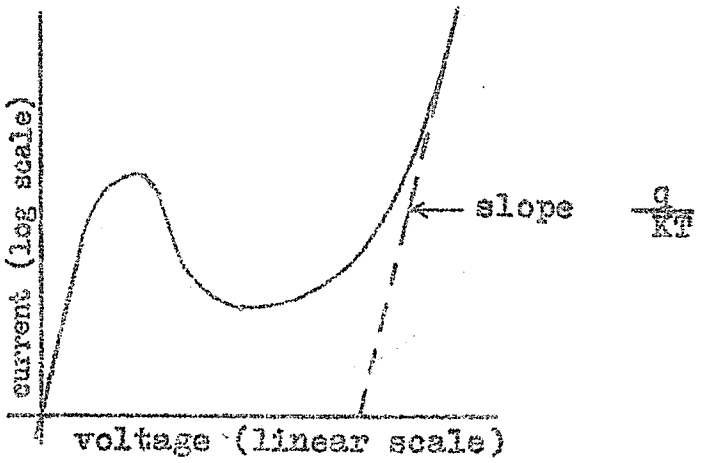

Figure 2.7 Semilogarithmic characteristic of the tunnel diode.

Figure 2.8

Calculated junction currents of the tunnel diode 1N2939.

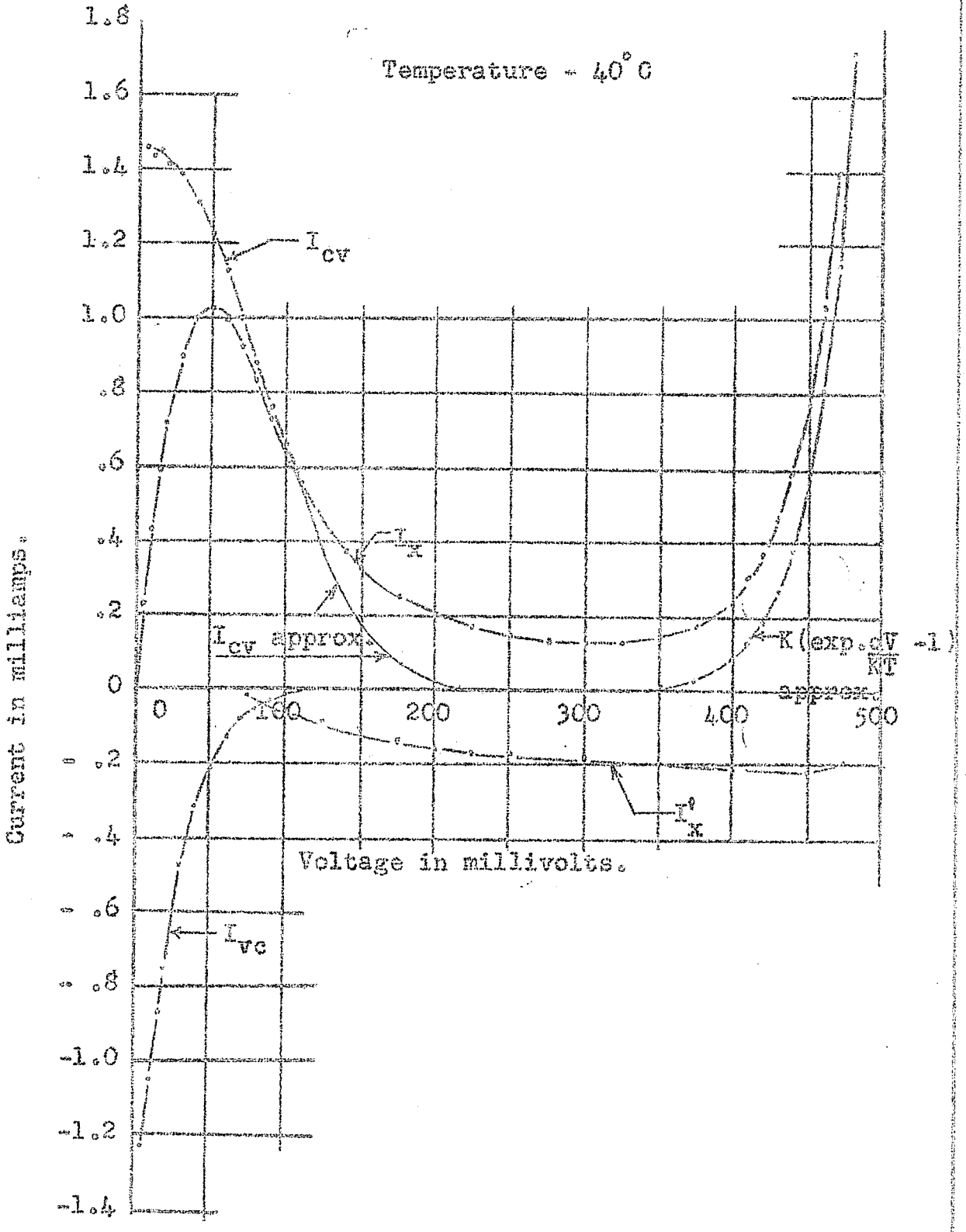

CHAPTER III

QUALITATIVE DESCRIPTION OF THE TUNNEL DIODE

SHOT NOISE CHARACTERISTICS

Chang was the first to report that the noise existing in the negative conductance region was shot noise.[3]* Tiemann later reported that the currents I_{cv}, I_{vc}, and I_x are completely uncorrelated.[4] By a similar argument I_f is uncorrelated with I_x since the mechanism of I_f is diffusion and the mechanism of I_x is tunneling.

I. SHOT NOISE DUE TO THE ZENER AND ESAKI CURRENTS

An expression for the sum of the Esaki and Zener currents may be obtained by the addition of equations 2.9 and 2.10.[8]

$$I_{cv} + I_{vc} = \frac{I_c'}{1-\exp.\ -\frac{qV}{KT}} + \frac{I_c'}{\exp \frac{qV}{KT} - 1} \quad \ldots\ldots\ldots\ldots \quad 3.1$$

By simplifying it follows that

$$I_{cv} + I_{vc} = I_c' \coth \frac{qV}{2KT} \quad \ldots\ldots\ldots\ldots\ldots\ldots\ldots\ldots \quad 3.2$$

This equation represents the average equivalent shot noise current due to the Esaki and Zener currents. However it must be noted that this equation is only applicable in the low bias region and a small portion of the negative conductance

---

* A detailed description of shot noise will be given in the fourth chapter.

region as seen from figure 2.5.

La Rosa and Wilhelmsen have advanced a theory of shot noise reduction in the negative conductance region.[11] They state that the eligible electrons have a finite probability of tunneling and consequently the diode is not as noisy as first assumed. The current I_{vc} produces full shot noise due to its infinitesimal probability, but the current I_{cv} is smoothed. The resultant equivalent noise current is equal to $\gamma^2 I_{cv}$ where γ^2 is the smoothing factor.

They derive the equation

$$\gamma^2 = 1 - Z_{cv} f_c (1-f_v)$$

where $Z_{cv} f_c(1-f_v)$ is the joint probability of c→v and v→c tunneling. At a sufficiently large forward bias

$$f_c \approx 1 - f_v \approx 1$$

hence $\gamma^2 = 1 - Z_{cv}$

The junction is degenerate so that the conduction electrons behave as a gas. The lowest energy electrons are responsible for the tunneling and since tunneling does not require a change of energy, the tunneling electrons are unaware of the potential hill. This would mean that there would be a 50% probability of heading through the thin junction. Based on this hypothesis Z_{cv} is assumed to have a value of 0.5 and the smoothing factor γ^2 is then calculated to be equal to 0.5.

Lee and Yariv present arguments that the tunneling mechanism of I_{cv} does not lead to shot noise smoothing.[12] Unfortunately, only the tunneled electron current can be

measured so that an actual tunneling probability can not be measured but only predicted. The predicted tunneling probabilities are much less than 50%. They state that the current may be considered to be a superposition of impulses occurring independently at random intervals, which in turn would produce full shot noise.

At thermal equilibrium the shot noise due to I_{cv} and I_{vc} reduces to the thermal noise formula.[8] Equating the mean square noise currents for shot noise and thermal noise* an expression can be obtained for I_{cv} and I_{vc}.

$$2q(I_{cv} + I_{vc})B = \frac{4KTB}{R} \quad \ldots\ldots\ldots\ldots\ldots\ldots\ldots\ldots \quad 3.3$$

R is considered to be the dynamic impedance of the tunnel diode which can be expressed as

$$R = \left(\frac{\partial V}{\partial I_c'}\right)_{V=0} \quad \ldots\ldots\ldots\ldots\ldots\ldots\ldots\ldots\ldots\ldots \quad 3.4$$

I_c' is the corrected current due to the parasitic resistance of the diode. The current $(I_{cv} + I_{vc})$ expressed as the thermal equivalent is then

$$I_{cv} + I_{vc} = \frac{2KT}{q}\left(\frac{\partial I_c'}{\partial V}\right)_{V=0} \quad \ldots\ldots\ldots\ldots\ldots\ldots \quad 3.5$$

From equation 3.2

$$I_{cv} + I_{vc} = \frac{I_c'}{\tanh \frac{qV}{KT}} \quad \ldots\ldots\ldots\ldots\ldots\ldots\ldots \quad 3.6$$

When V reduces to zero, I_c' also reduces to zero. By taking the partial derivative, with respect to V, of the

---

* Thermal noise is described in detail in the fourth chapter.

numerator and denominator on the right hand side of expression 3.6, the current is then

$$I_{cv} + I_{vc} \xrightarrow[V \to 0]{} \frac{\frac{\partial I_c'}{\partial V}}{\frac{\partial \tanh \frac{qV}{KT}}{\partial V}} \qquad \ldots\ldots\ldots\ldots\ldots\ldots\ldots\ldots 3.7$$

$$= \left(\frac{\partial I_c'}{\partial V}_{V=0}\right) \frac{2KT}{q}$$

This expression is identically equal to equation 3.6.

From equation 3.3 it can be seen that $(I_{cv}+I_{vc})$ is directly proportional to the absolute temperature. It should be noted that at an absolute temperature of zero degrees, $(I_{cv}+I_{vc})$ will be equal to zero.

II. SHOT NOISE DUE TO THE EXCESS CURRENT

The excess current is considered to exhibit full shot noise. There now appears to be experimental evidence that noise greater than shot noise exists in the valley region. This additional noise may be theoretically justified for the following two reasons.

1. The noise may exceed the shot noise value by a measurable amount if the bound states have a lifetime less than about 2×10^{-9} seconds.[4]

2. A possible opposite current which is uncorrelated with I_x may exist due to the tunneling of electrons from the p-type to the n-type semiconductor for a voltage bias in the valley region. Although the existence of a reverse

current is possible. Agouridis and van Vliet consider it unlikely.[13]

Excess noise existing in semiconductors at low frequencies will be briefly described in the fourth chapter.

III. SHOT NOISE DUE TO THE CURRENT I_f

The noise existing in the tunnel diode at a large forward bias can be considered the same as the shot noise associated with the forward and reverse current of the conventional diode. From expression 2.11 the forward current is equal to $Ke^{\frac{qV}{KT}}$ and the reverse current is equal to K for the conventional diode. Both the forward and reverse currents are assumed to be completely uncorrelated.[21a] Therefore the equivalent shot noise current I_f of a conventional diode is

$$I_f' = K\left(e^{\frac{qV}{KT}} + 1\right) \quad \text{..... 3.8}$$

In the high forward bias region the variable $e^{\frac{qV}{KT}}$ is much greater than 1 and consequently the current I_f' is essentially equal to I_f.

CHAPTER IV

PHYSICAL SOURCES OF NOISE

Various sources of noise, such as resistors, semiconductors and vacuum diodes, are outlined in this chapter. Special attention is given to the generation of thermal noise in resistors and shot noise in vacuum diodes, since these provide a noise reference for the noise measurement of the tunnel diode.

I. NOISE ASSOCIATED WITH RESISTANCE

Thermal Noise

A resistor with no average current flowing through it has a fluctuating voltage across it because of the random thermal motion of electrons inside it. The average value of the voltage is zero but a certain average power is generated. The mean square voltage across the resistor is given as

$$\overline{v_t^2} = 4KTRB \quad \ldots\ldots\ldots\ldots\ldots\ldots\ldots\ldots \quad 4.1$$

where K is the Boltzmann constant equal to 1.38×10^{-23} joules/^{o}C; T is the temperature in degrees Kelvin; R is the resistance in ohms; B is the noise bandwidth in cycles per second.

The experimental data for thermal noise was first given by Johnson[14] and the theoretical derivation was given later by Nyquist.[15]

The spectrum of thermal noise is white noise. In other words, the energy density spectrum is a horizontal straight line when plotted against frequency if the resistor is assumed to remain purely resistive over this frequency. This is illustrated in figure 4.1.

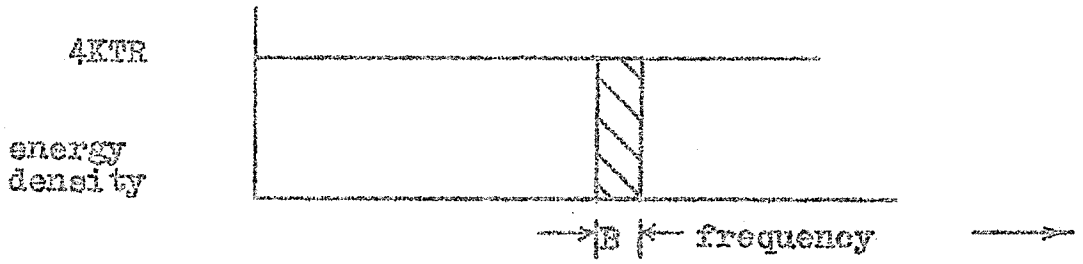

Figure 4.1 Energy density spectrum.

The crosshatched portion represents the fluctuation energy in frequency band B.

It is to be noted that the noise bandwidth B is not the same as the 3db bandwidth.[23] The noise bandwidth B is considered to be the bandwidth of an idealized bandpass characteristic having the same total area and peak value as the power versus frequency curve of the amplifier. The factor relating the noise bandwidth B and the 3db bandwidth can be determined.

A sample of thermal noise indicating its Gaussian behaviour is shown in figure 4.2

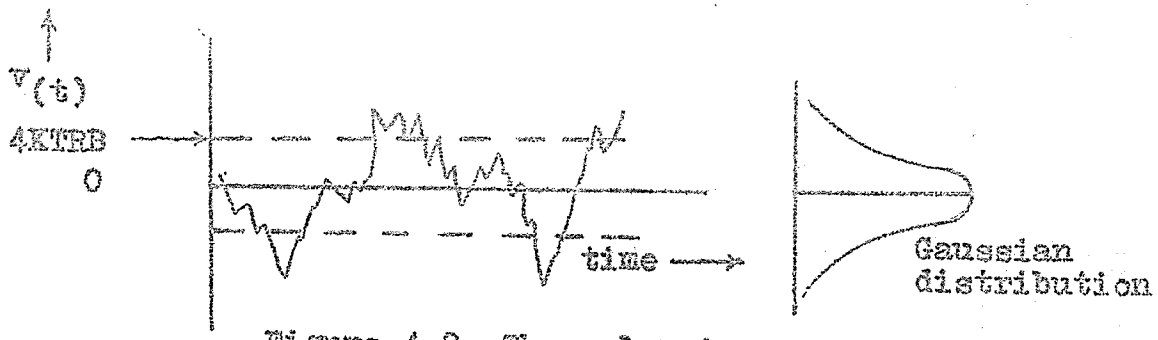

Figure 4.2 Thermal noise

An eventual "drop-off" of the noise spectrum is to be expected since an infinite flat spectrum would imply infinite noise energy generation. The expression for thermal noise for high frequencies is given by Nyquist as[21b]

$$\overline{v_t^2} = \frac{4hfRB}{\frac{hf}{KT} - 1} \qquad \text{4.2}$$

where h is Planck's constant equal to 6.62×10^{-34} joule-seconds. At a frequency of 10 gigacycles per second the difference in value between expressions 4.1 and 4.2 is less than 1%.

Thermal Noise Representation

The thermal noise may be represented either as a voltage or current generator. These alternative representations are shown in figure 4.3.

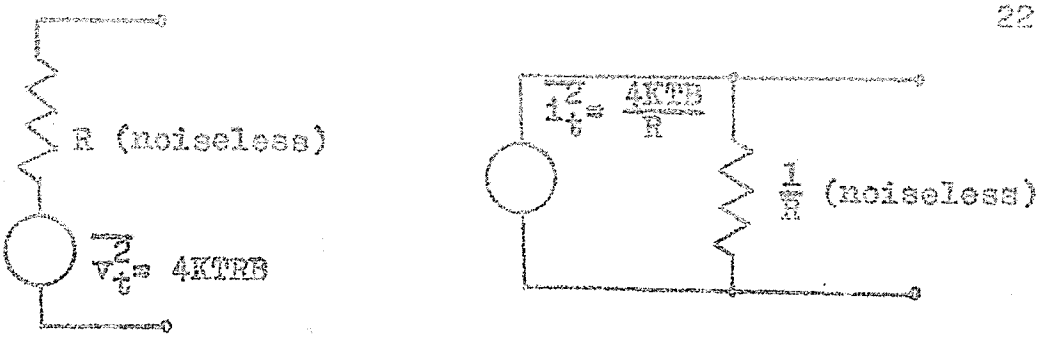

(a) voltage generator (b) current generator

Figure 4.3 Representation of thermal noise.

If the resultant noise of more than one resistor is required, the noise generation of each resistor must be considered completely uncorrelated and consequently the squared noise voltages or currents must be added. Figure 4.4 illustrates this principle.

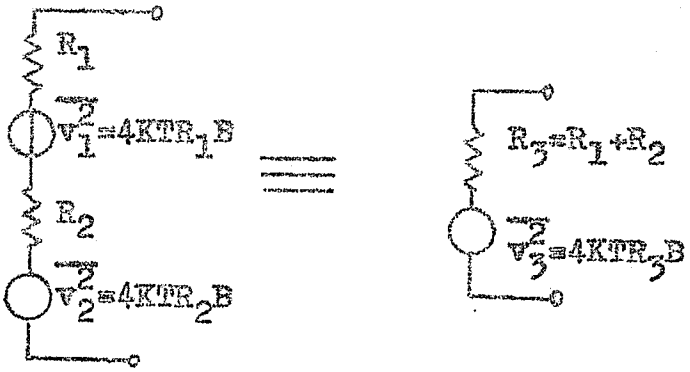

(a) voltage generator

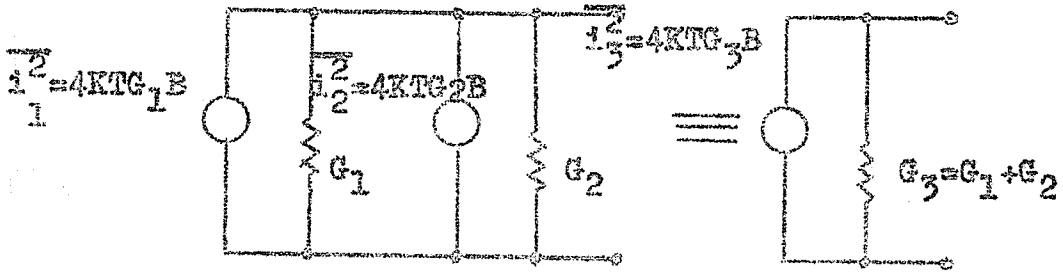

(b) current generator

Figure 4.4 Representation of the summation of thermal noise.

The contribution of noise due to a one megohm grid-leak resistor at the input of the first stage of an amplifier is negligible for a signal source impedance of 50 ohms.[26a]

Contact Noise

In addition to thermal noise, contact noise is known to be generated in granular resistors. Contact noise may be adequately expressed as [21c]

$$\overline{i_c^2} = \frac{KI^a B}{f^b} \qquad \ldots\ldots\ldots\ldots\ldots\ldots\ldots\ldots\ldots\ldots 4.3$$

where I is the average current passing through the resistor; f is the frequency; a and b are constants approximately equal to 2 and 1 respectively. By considering a number of contacts in parallel and a number of contacts in series, it can be shown that the contact noise is inversely proportional to the volume and particle density of the granular resistor. On this basis, thin layer granular resistors and carbon microphones exhibit a relatively large amount of noise. Contact noise is assumed negligible above 100 kilocycles per second.[25a]

Christenson and Pearson made noise measurements on a solid graphite* bar and were unable to detect any contact noise inherent in the solid carbon.[10] Solid metallic resistors like the wire-wound type do not generate any measurable amount of contact noise.

---

*Graphite is considered to be a conductor, not a semiconductor.

Shot Noise

Shot noise is considered to exist in a resistor only as a second order effect.[21d] The argument presented by A. van der Ziel is as follows.

The number of free electrons in the conduction band is fixed. This then prevents any shot noise from being generated according to the shot noise argument for semiconductors. However, the contribution of an electron to the resistance depends on its energy E. Since the electrons are moving at random, the number of electrons having an energy between E and E + E does not remain fixed. It is therefore expected that a small fluctuation in resistance does exist as a second order effect.

II. NOISE ASSOCIATED WITH VACUUM DIODES

Shot Noise

The generation of shot noise in a diode will be considered for the temperature limited case only. The current in a diode is due to an electron flow from the cathode to the plate. Electrons arriving at the plate will fluctuate around an average value with respect to time. In a temperature limited diode in which all the emitted electrons arrive at the plate, the mean square noise current due to the fluctuations is given as

$$\overline{i_s^2} = 2qI_dB \quad \ldots\ldots\ldots\ldots\ldots\ldots\ldots\ldots\ldots\ldots \quad 4.4$$

where I_d is the average current flow in the diode.

A sample of shot noise is shown in figure 4.5.

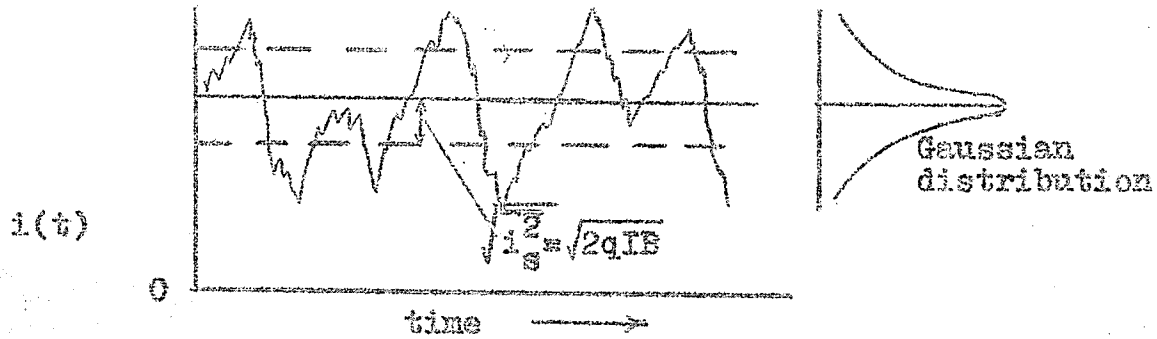

Figure 4.5 Shot noise.

Shot noise is also considered to have a Gaussian distribution.

At high frequencies the shot noise is reduced because of the transit time effect. The reduction factor is given by van der Ziel[21e] as

$$1 - \frac{1}{18} W^2\tau^2 + \ldots \qquad 4.5$$

where W is the frequency in radians per second and τ is the electron transit time. The transit time is directly proportional to the distance between the plates and inversely proportional to the square root of the plate voltage.

The transit time effect can therefore be reduced by decreasing the distance between the plates although this has the undesirable effect of increasing the capacitance. Also, a large plate voltage is desirable in reducing the transit time error.

The general "rule of thumb" used for the calculation

of the noise cut-off frequency f_c is that f_c is equal to the reciprocal of the transit time. For the space charge limited diode the noise is substantially smoothed due to the presence of the space charge near the cathode.

Representation of Diode Shot Noise

If the reactance and the transit time effects are assumed negligible then the diode shot noise may be represented by a single current generator of infinite impedance as shown in figure 4.6.

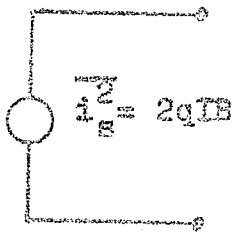

Figure 4.6 Representation of shot noise.

If the series inductance and interelectrode capacitance are taken into account then the mean square noise current is reduced by the following factor.

$$\frac{1}{1 - W^2LC} \quad \ldots\ldots\ldots\ldots\ldots\ldots\ldots\ldots \quad 4.6$$

Flicker Noise

At low frequencies the diode exhibits greater noise than that of shot noise alone. This noise, called flicker noise, is similar to the contact noise in resistors and can also be described by expression 4.3.

Flicker noise is known to vary greatly between diodes of equal dimensions. It is attributed to slow variations of the cathode surface and therefore is only present at low frequencies. Aged diodes exhibit a greater noise because of a coating formed on the cathode. Flicker noise is assumed to be negligible above 1.0 megacycle per second.[25a]

Diode Used as a Noise Generator

The type 5722 diode is designed for noise application use.[27] This tube may be employed for use as a noise generator up to 100 megacycles per second without any appreciable error due to the transit time effect. The circuit diagram for the noise generator is shown in figure 7.3. For the procedure used for the noise measurements, the interelectrode capacitance is negligible. The reactance due to the lead inductance is partially cancelled by the negative reactance of the blocking capacitor C_1.

The low pass filter composed of C_3, C_4, C_5, C_6, L_1, L_2, L_3 and L_4 serves as a blocking device for all extermal noise entering the input system from the power supply. The value of R_1 is large so that the thermal noise generated by it will be almost negligible when measuring the thermal noise of a resistor less than 100 ohms in parallel with it.

With 150 volts applied to the plate, the diode is in a temperature-limited condition. The voltage of the battery is varied from zero to as much as is required to produce

the desired amount of noise output.

III. SEMICONDUCTOR NOISE

Semiconductors are known to generate thermal noise which is associated with their internal resistance. Shot noise and excess noise on the other hand are associated with the current drift through the semiconductor.

The generation of shot noise and excess noise stems from the fact that the number of electrons in the conduction band is constantly changing. This gives rise to a changing effective resistance. The slow variations give rise to the excess noise and the other variations give rise to the shot noise. Noise generated in germanium has been experimentally investigated by Herzog, Mattson, and van der Ziel.[16] Excess noise was found to exist up to 10 megacycles per second.

Excess noise, being similar in nature to contact and flicker noise, can also be expressed by equation 4.3. Shot noise exists only in semiconductors of high resistivity. A highly doped semiconductor has a sufficient number of electrons in the conduction band except at very low temperatures.

CHAPTER V

EQUIVALENT CIRCUIT OF THE TUNNEL DIODE

The tunnel diode exhibits a small amount of thermal noise which can be attributed to its internal resistance. The contribution of the thermal noise to the total noise generated depends on the dynamic impedance of the tunnel diode. In this chapter by means of the equivalent noise circuit, the effect of the parasitic resistance will be shown.

I. EQUIVALENT CIRCUIT

The standard small signal equivalent circuit of the tunnel diode is shown in figure 5.1

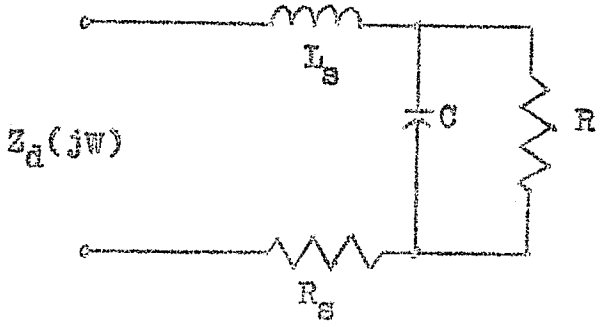

Figure 5.1 Equivalent circuit of the tunnel diode.

The resistance R may be positive or negative, depending on the bias voltage. It can be determined approximately if the dynamic impedance $Z_d(jW)$ is known and if the admittance of C and L are small.

The shunt capacitance C is composed of the junction capacitance and the external case and lead capacitance. C is known to vary with the bias voltage and must therefore be considered at a particular bias point. A V.H.F. bridge can be used for the measurement of C.

The inductance L_s can be considered as external to the p-n junction and is due to the package and lead length only.

The series resistance R_s is the internal resistance of the tunnel diode and is the bulk resistance of the semiconductor material. The value of R_s can be determined by measuring the dynamic impedance at large negative bias currents.[28]

II. EQUIVALENT NOISE CIRCUIT

Figure 5.2 shows the equivalent noise circuit of the tunnel diode.[29] $\overline{v_t^2}$ represents the thermal noise associated with the resistance R_s and $\overline{i_s^2}$ represents the shot noise associated with the junction of the diode. I_{eq} is the equivalent shot noise current as given in expression 1.2.

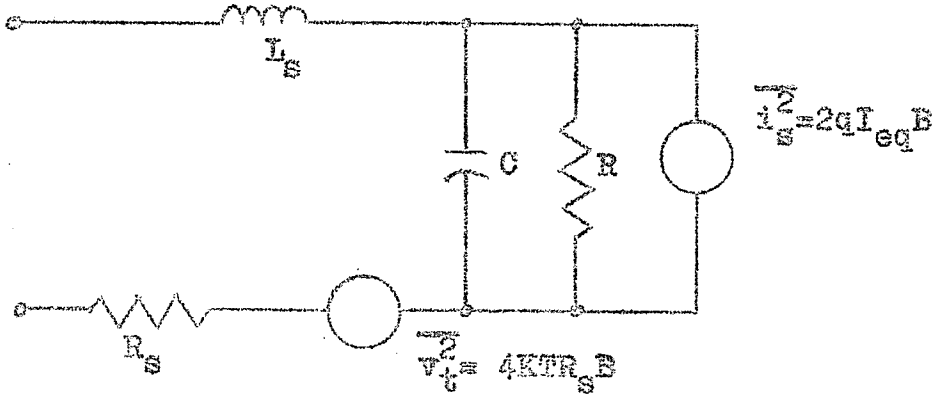

Figure 5.2 Equivalent noise circuit.

The series equivalent noise circuit which is obtained by simple calculation is shown in figure 5.3.[29]

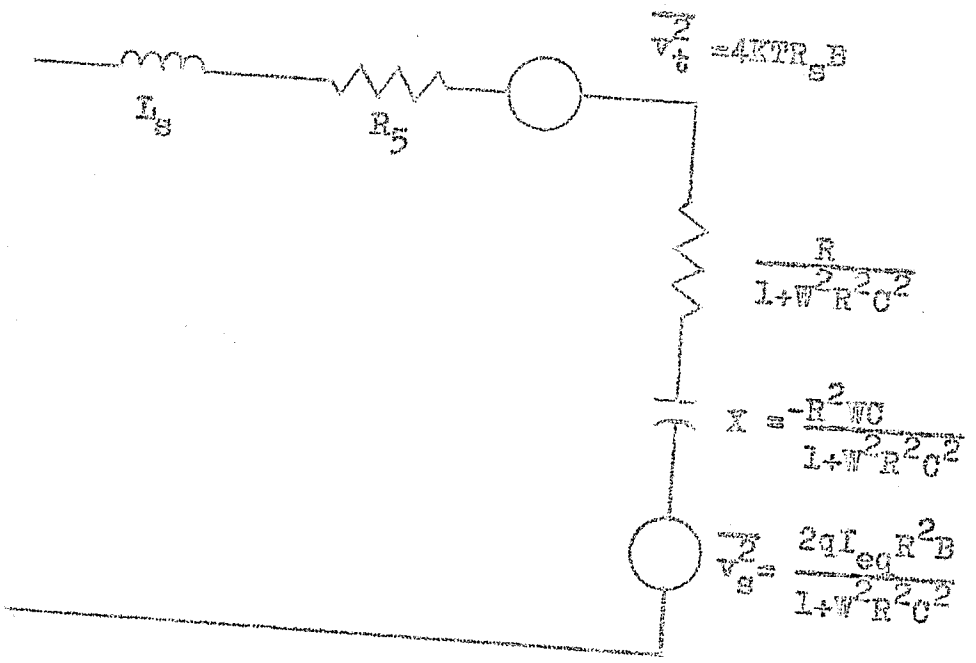

Figure 5.3 Series equivalent noise circuit.

The tunnel diode shunt equivalent noise circuit shown in figure 5.4 is found by taking the Norton equivalent of the series equivalent noise circuit.

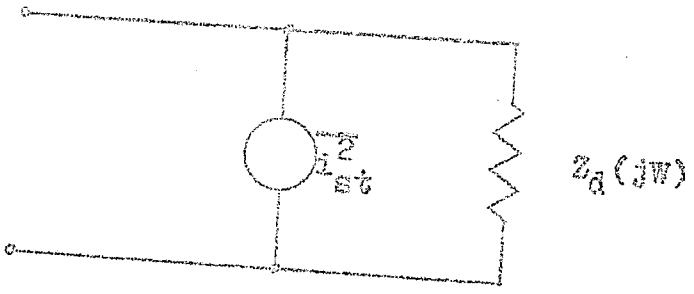

Figure 5.4 The shunt equivalent circuit.

$Z_d(jW)$ is the dynamic impedance of the tunnel diode. The shunt mean square current $\overline{i^2_{s+}}$, due to the shot and thermal noise, may be expressed as

$$\overline{i^2_{st}} = \frac{4KTR_sB + \frac{2qI_{eq}R^2B}{1+W^2R^2C^2}}{\left(R_s + \frac{R}{1+W^2R^2C^2}\right)^2 + \left(WL_s - \frac{R^2WC}{1+W^2R^2C^2}\right)^2} \quad \ldots\ldots\ldots 5.1$$

$$= 2qI'_{eq}B \quad \ldots\ldots\ldots 5.2$$

$$\text{where } I'_{eq} = \frac{\frac{2KTR_s}{q} + \frac{I_{eq}R^2}{1+W^2R^2C^2}}{\left(R_s + \frac{R}{1+W^2R^2C^2}\right)^2 + \left(WL_s - \frac{R^2WC}{1+W^2R^2C^2}\right)^2} \quad \ldots\ldots 5.3$$

III. THE EFFECT OF R_s AND L_s

The calculated shot noise of the tunnel diode neglects the series inductance and resistance. In this section the effect of R_s and L_s on the tunnel diode noise generation will be outlined.

If R_s and L_s are neglected in the circuit in figure 5.2 then the total equivalent noise current generated by the tunnel diode is I_{eq}. However, if R_s and L_s are taken into account as in the circuit in figure 5.4 then the calculated equivalent noise current is I'_{eq}. For frequencies of 30 and 60 megacycles per second the greatest difference between I'_{eq} and I_{eq} will occur when R is small. The two regions in

which this occurs are at zero bias and at a large forward bias.

The dynamic impedance of the tunnel diode was found to be approximately 20 ohms at zero bias. For this condition I'_{eq} can be calculated by substituting the following values into equation 5.3.

T = 313° Kelvin
R = 18.5 ohms (at zero bias)
R_s = 1.5 ohms
C^s = 5 pf.
L_s = 6 nh.
W = 2π30 x 10^6 radians per second
I_{eq} = 2,840 microamps (From figure 7.8 at zero bias)

The value for I'_{eq} was calculated to be equal to 2,630 microamps which corresponds to a value of 210 microamps less than the value for I_{eq}. This difference decreases rapidly for a positive increase in bias and is almost non-existant in the negative conductance region. The measured equivalent noise current from figure 7.8 at zero bias is 2,720 microamps which is 90 microamps above the value for I'_{eq}.

Due to the variable $\coth \frac{qV}{2KT}$, in equation 3.2, the value of I_{eq} can be calculated only within a limited accuracy at zero bias. The variable $\coth \frac{qV}{2KT}$ in the limit increases to an infinite value when V decreases to zero. It is therefore felt that calculations for the values of I'_{eq} would not be justified.

CHAPTER VI

STABILITY CRITERION

In order to obtain noise measurements and the current-voltage characteristic of the tunnel diode, it is necessary to stabilize it in the negative conductance region. Stabilization is accomplished by connecting external circuit elements to the terminals of the tunnel diode. In this chapter the stability of the circuit containing the tunnel diode and the external elements, will be examined by means of the Hurwitz stability criterion.

I. PARALLEL CONFIGURATION OF THE TUNNEL DIODE AND RESISTOR

The equivalent circuit of the tunnel diode, for a bias voltage in the negative conductance region, is shown in figure 6.1.

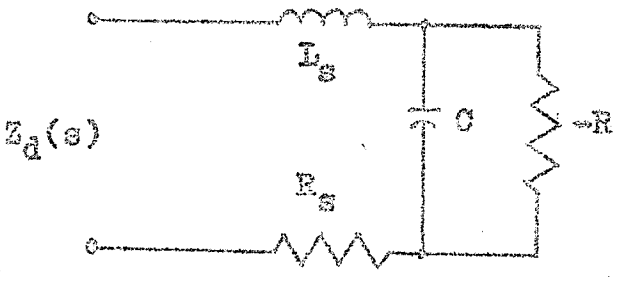

Figure 6.1 Equivalent circuit of the tunnel diode.

The complex input impedance $Z_d(S)$ of the tunnel diode can be calculated to be equal to the following

$$Z_d(S) = \frac{S^2 L_s C + S(R_s C - L_s/|R|) + (1-R_s/|R|)}{SC-1/|R|} \quad \ldots\ldots\ldots \quad 6.1$$

The type of stability to be considered in this chapter is that of placing a resistor having impedance $Z_R(S)$ across the terminals of the tunnel diode. The expression for $Z_R(S)$ is

$$Z_R(S) = R_R + SL_R \quad \ldots\ldots\ldots\ldots\ldots\ldots\ldots\ldots\ldots \quad 6.2$$

where R_R is the resistance and L_R is the series lead inductance of the resistor.

Figure 6.2 shows the parallel configuration of the resistor and the tunnel diode.

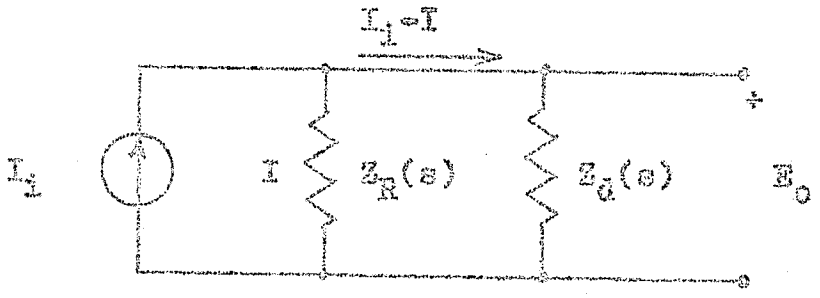

Figure 6.2 Parallel configuration of $Z_R(S)$ and $Z_d(S)$.

I_1 is the input current signal and E_o is the corresponding output voltage.

II. APPLICATION OF THE HURWITZ STABILITY CRITERION

The purpose of this section is to determine the required condition of $Z_R(S)$ in order to stabilise the circuit

shown in figure 6.2. A linear circuit is considered stable if and only if its output, in response to every bounded input, remains bounded.[18] It is then required to show that for a bounded input current I_i the resultant output voltage E_o remains bounded.

In order to apply the Hurwitz stability criterion it is necessary to represent the circuit shown in figure 6.2 as a feedback system. The block diagram of the feedback system is shown in figure 6.3.

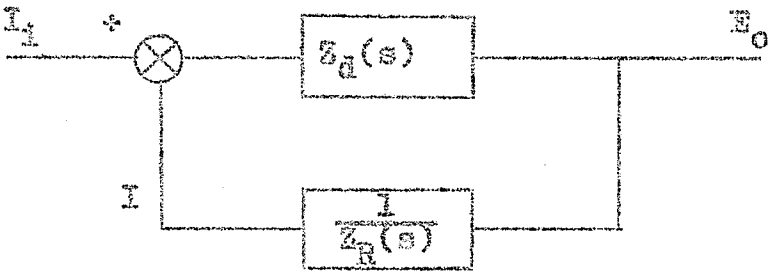

Figure 6.3 Block diagram of the feedback system.

The open loop gain A(S) of the feedback system is

$$A(S) = \frac{Z_d(S)}{Z_R(S)} \qquad \ldots\ldots\ldots\ldots\ldots\ldots\ldots\ldots \quad 6.3$$

The transfer function of the complete system is

$$\frac{E_o}{I_i} = \frac{Z_d(S)}{1 + A(S)} \qquad \ldots\ldots\ldots\ldots\ldots\ldots\ldots\ldots \quad 6.4$$

The characteristic equation may be obtained by equating 1 + A(S) to zero. From equation 6.3 it follows that

$$Z_R(S) + Z_d(S) = 0 \qquad \ldots\ldots\ldots\ldots\ldots\ldots\ldots\ldots\ldots\ldots\ldots\ldots \quad 6.5$$

The sum of $Z_R(S)$ and $Z_d(S)$ is of the same form as equation 6.1 and therefore

$$Z_R(S) + Z_d(S) = \frac{S^2 L_T C + S(R_T C - L_T/|R|) + 1 - R_T/|R|}{SC - 1/|R|} \quad .. \quad 6.6$$

where $R_T = R_S + R_R$ 6.7

and $L_T = L_S + L_R$ 6.8

The characteristic equation is then

$$S^2 L_T C + S(R_T C - L_T/|R|) + 1 - R_T/|R| = 0 \quad ..... \quad 6.9$$

The Hurwitz criterion states that for stability all the coefficients of the characteristic equation must have the same sign and that all its determinants must be positive.

The first condition requires that

$$R_T C - L_T/|R| > 0 \quad ..... \quad 6.10$$

and $$1 - R_T/|R| > 0 \quad ..... \quad 6.11$$

The second condition requires

$$D_1 = L_T C > 0 \quad ..... \quad 6.12$$

and $$D_2 = \begin{vmatrix} R_T C - L_T/|R| & 1 - R_T/|R| \\ 0 & L_T C \end{vmatrix} > 0 \quad ..... \quad 6.13$$

Expression 6.13 is identical to expression 6.11 and consequently the condition for stability is

$$|R| > R_T > \frac{L_T}{|R|C} \quad ..... \quad 6.14$$

Other forms of stabilization may also be used.[20]

CHAPTER VII

NOISE MEASUREMENTS

Noise measuring systems usually consist of a high-grain linear amplifier and a detector.[3,4,17] Some detectors are designed to be either purely linear or quadratic while others may behave in some other nonlinear manner. For a receiver containing a linear detector and amplifier, the output voltage is linearly dependent on the input voltage. If, however, a quadratic detector is used in conjunction with a linear amplifier, then the output reading is proportional to the input power. When performing the tunnel diode noise measurements the input impedance and signal level to the preamplifier were held constant. It is therefore neither required that the detector be linear or quadratic, nor is it necessary for the amplifier to be linear.

I. NOISE MEASUREMENTS AT 30 MEGACYCLES PER SECOND

Procedure

In order to measure the tunnel diode shot noise it is necessary to choose a frequency at which the excess noise of the tunnel diode is negligible. The generation of excess noise in a tunnel diode can generally be assumed negligible at 30 megacycles per second although excess noise existing up to 50 megacycles per second has been reported.[30] Flicker noise and contact noise are negligible at 30 megacycles

per second and therefore the shot noise generated in vacuum diodes and the thermal noise generated in carbon resistors can be used as noise standards. A low-noise 30 megacycles per second receiving system was available, facilitating the noise measurements at this frequency. Also, the test frequency at 30 megacycles per second is low enough so that the tunnel diode noise measurement error due to its own capacitance is negligible.

The block and schematic diagrams for noise measurement at 30 megacycles per second are given in figures 7.1 and 7.2 respectively. The noise signal is provided by the noise generator, the schematic of which is shown in figure 7.3. The noise generator was connected to the preamplifier with the shortest possible leads, thereby minimizing the lead inductance and stray pickup effect. Precautions were taken to prevent any external 30 megacycles per second signal from entering into the receiving system at the input. The noise generator includes a low-pass filter isolating the diode 5722 from the power supply. A low-pass filter consisting of elements C_2, C_3 and L_3 in figure 7.2 prevents any stray 30 megacycle per second signal from entering into the input from the tunnel diode bias supply.

In order to maintain an equal loading of the input impedance during a set of noise measurements, it is necessary that the impedance of the components placed across terminals $X - X^1$ be equal. This is achieved by the use of the 30 mega-

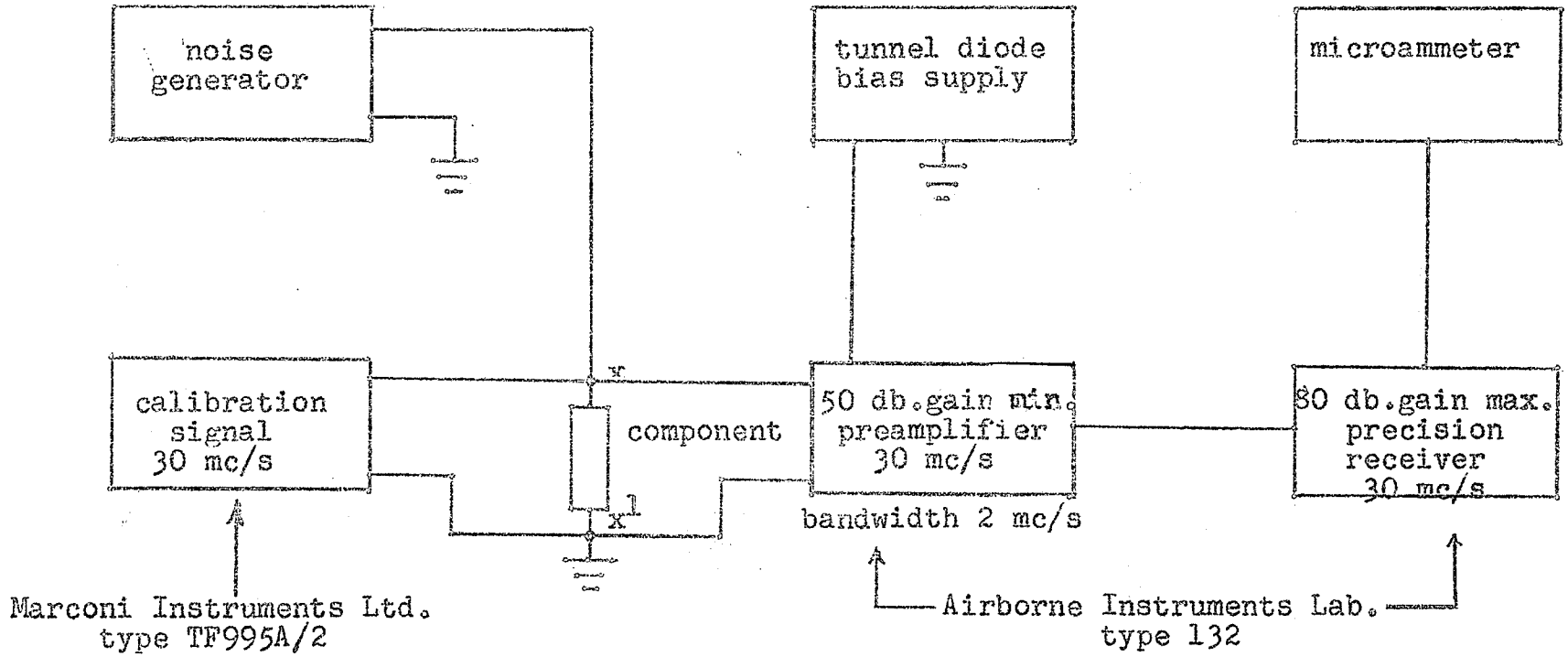

Figure 7.1

Block diagram of noise measurement circuit

at 30 megacycles per second.

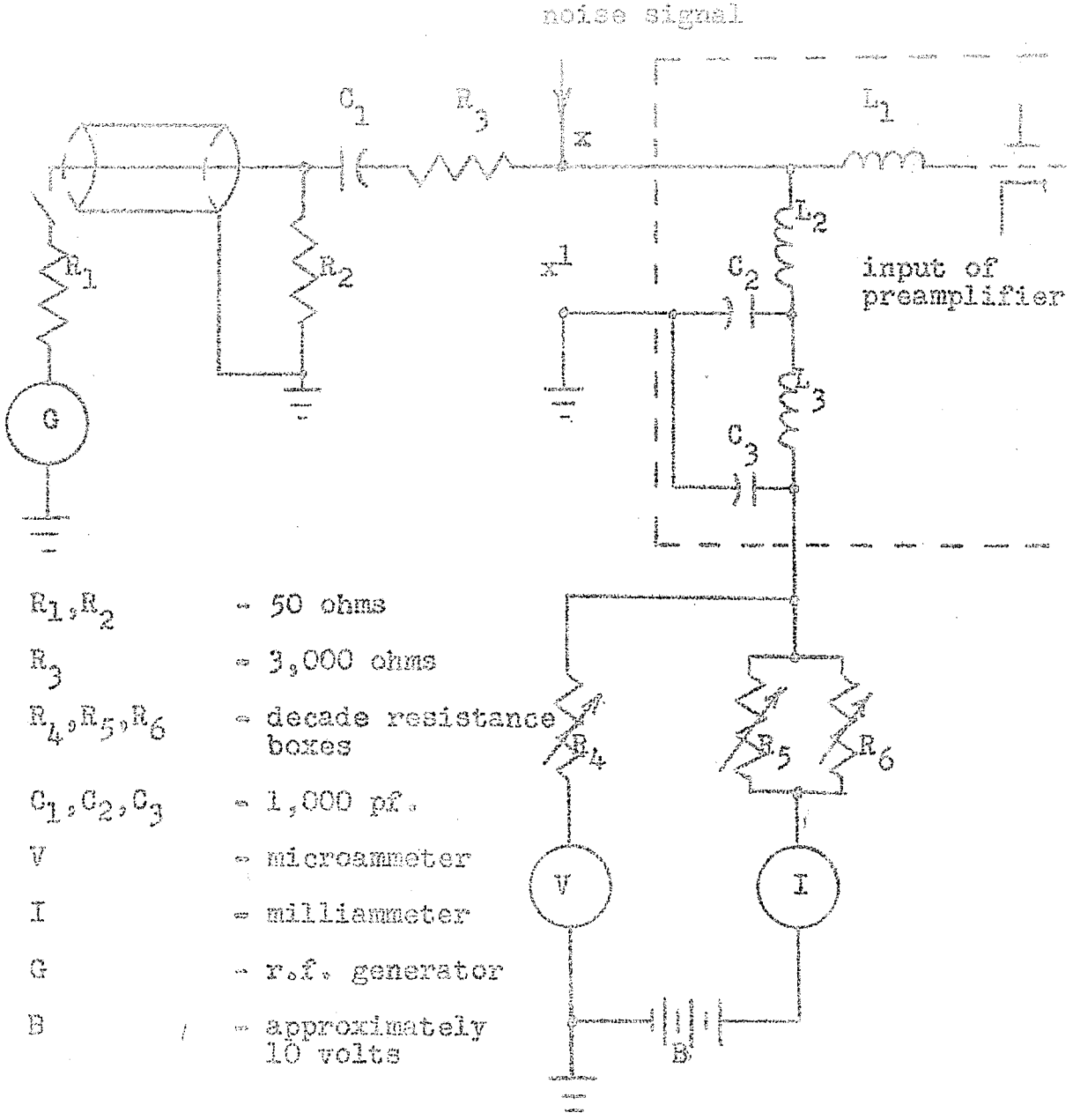

Figure 7.2

Schematic diagram of noise measurement circuit at 30 megacycles per second.

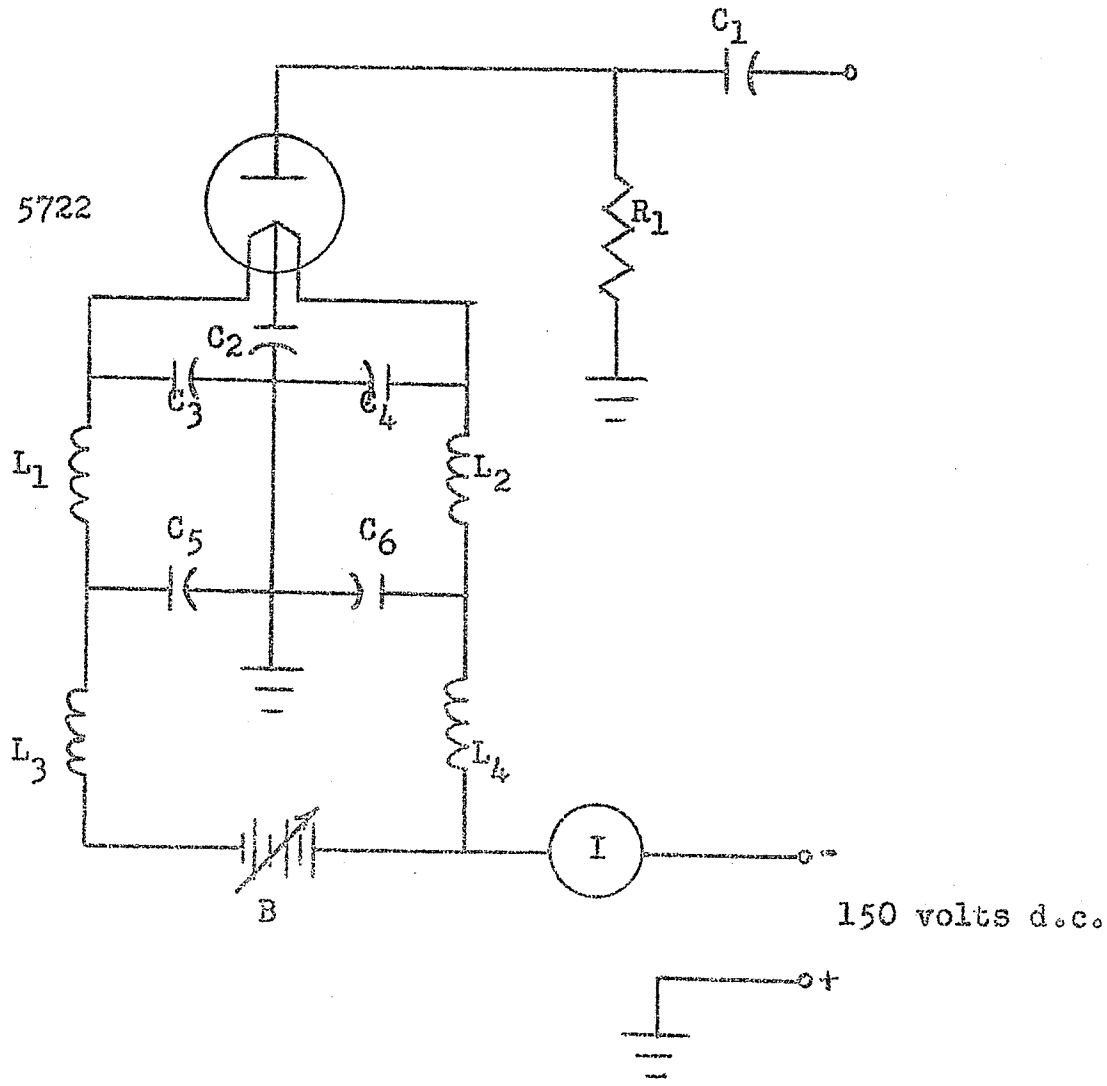

$C_1, C_2, C_3, C_4, C_5, C_6$	- 1,000 pf.
R_1	- 1,000 ohms
L_1, L_2	- 10 turns 3/16 inch diameter
L_3, L_4	- 45 turns 3/8 inch diameter
B	- 0-6 volts, 2 amps.
I	- milliammeter
5722	- Sylvania noise diode

Figure 7.3

Circuit diagram of noise generator.

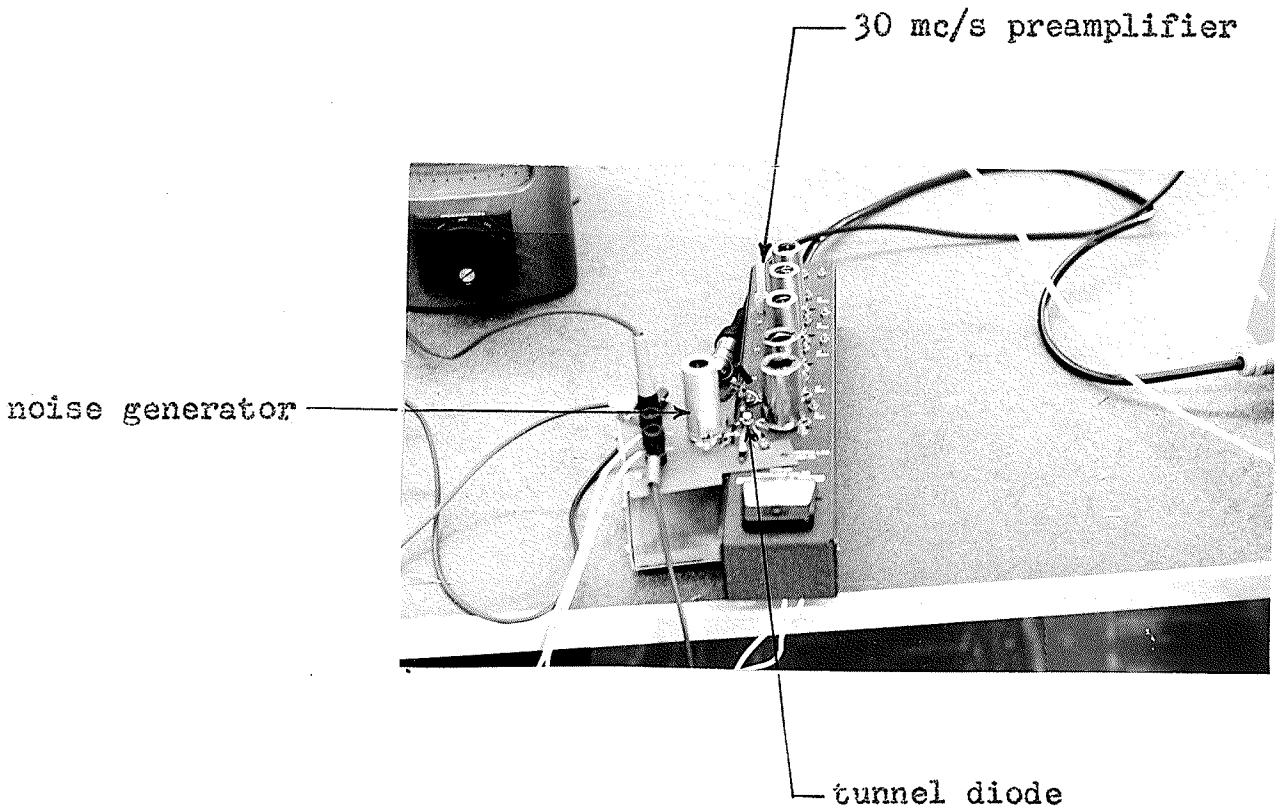

Figure 7.4

Input system of the 30 megacycles per second receiving system.

cycles per second calibrating signal. A resistor* of suitable impedance is inserted into the circuit across the terminals X - X^1. With the filament of the noise generator switched off, the calibrating signal is applied to the input circuit. The value of the signal is of sufficient magnitude to swamp out any inherent noise of the input system. At the same time it must be remembered not to exceed a signal level which would cause serious nonlinear effects when the dynamic impedance of the tunnel diode is being adjusted. The receiver output meter deflection M_s is noted. The resistor across X - X^1 is now replaced by the tunnel diode. Maintaining the same calibrating signal level, the bias of the tunnel diode is varied until the same deflection M_s is again read on the output meter. The dynamic impedance of the tunnel diode is then equal to the impedance of the resistor. The reverse procedure was not used since a variable high frequency resistor was not available. For the negative conductance region the procedure is slightly modified because of the stabilizing resistor used in parallel with the tunnel diode.

The noise generated by the tunnel diode and the resistors varies with temperature; consequently an accurate temperature measurement at the input of the preamplifier is required. Due to the proximity of the components to the preamplifier, their temperature was above room temperature. The following procedure was used to determine the temperature of the components connected across X - X^1. A tunnel diode

*The type of resistors used throughout were 0.25 watt carbon composition.

current-voltage characteristic was measured with the tunnel diode connected across X - X^1. This current-voltage characteristic was then compared with the temperature calibrated current-voltage characteristic curves given in figure A.2 of the appendix. In this manner, the temperature of the component connected across X - X^1 could be established within reasonable accuracy, since the current-voltage characteristic of the diode varies substantially for a small change in temperature.

Figure 7.4 is a photograph showing the input system of the 30 megacycles per second test setup.

The equivalent noise circuit of the input system is shown in figure 7.5.

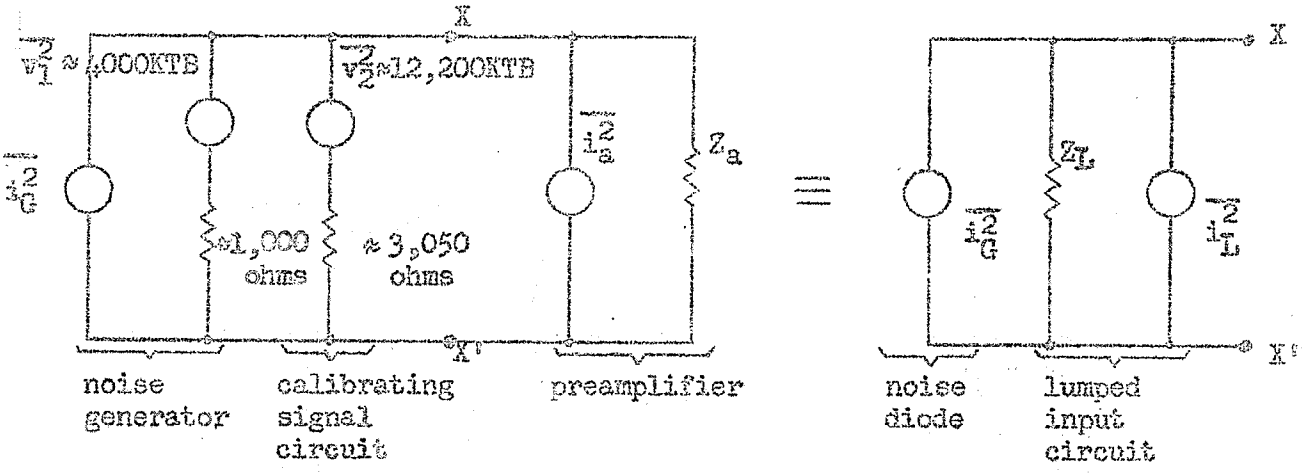

Figure 7.5 Noise equivalent circuit of the input system

In figure 7.5 $\overline{i_a^2}$ represents the noise contribution and Z_a represents the impedance of the amplifier. The impedance of the noise generator and calibrating signal circuit impedance can be lumped together respectively with $\overline{i_a^2}$ and Z_a to

give a resultant mean square noise current of i_L^2 and a resultant impedance Z_L.

Noise measurement in the positive conductance region

With the calibrating signal switched off and with the tunnel diode at a set bias in the positive condance region connected across X - X^1, a deflection M_d is obtained on the output meter. The tunnel diode is then replaced by the resistor which was previously determined to have an equal dynamic impedance to the tunnel diode at the set bias value. The filament supply of the noise diode is then varied until a deflection M_d is again obtained. The plate current I_G of the noise diode is accurately noted.

Figures 7.6 and 7.7 show the schematic diagrams of the total noise generated at the input circuit of the amplifier, with the components connected across the terminals X - X^1.

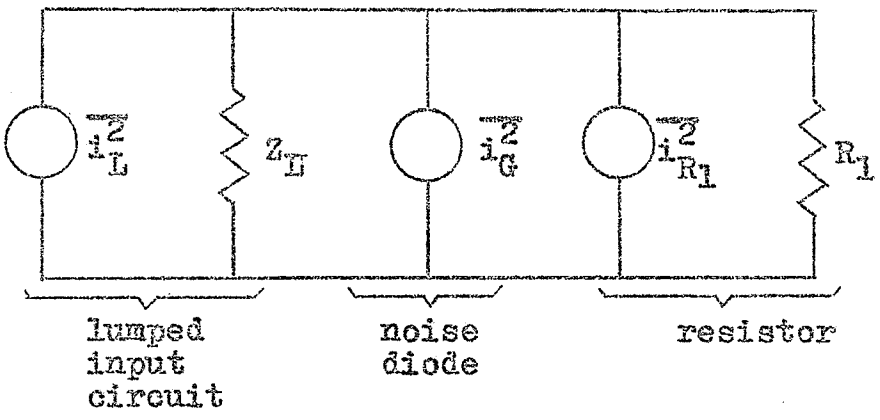

Figure 7.6 Noise schematic diagram of the input circuit containing the resistor and the noise diode.

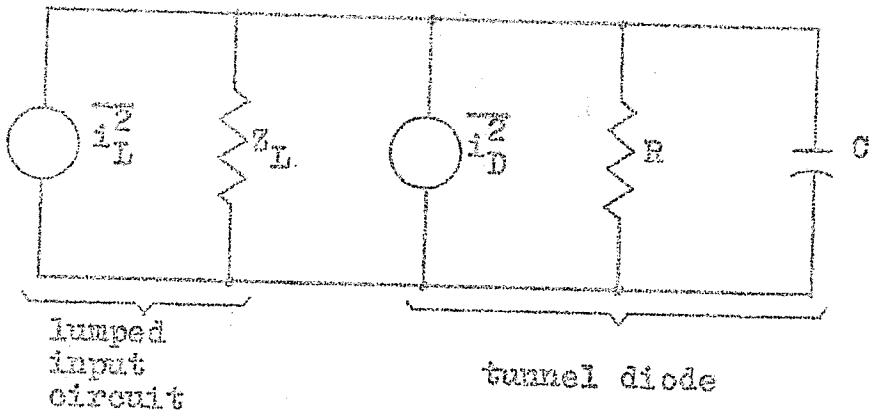

Figure 7.7 Noise schematic diagram of the input circuit containing the tunnel diode.

The series resistance R_s and inductance L_s of the tunnel diode are assumed negligible. The noise contribution of all sources at the input of the amplifier is the same in figures 7.6 and 7.7.

Therefore $$\overline{i_L^2} + \overline{i_D^2} = \overline{i_G^2} + \overline{i_{R_1}^2} + \overline{i_L^2} \quad \ldots\ldots\ldots\ldots\ldots\ldots \quad 7.1$$

Simplifying $$\overline{i_D^2} = \overline{i_G^2} + \overline{i_{R_1}^2} \quad \ldots\ldots\ldots\ldots\ldots\ldots\ldots\ldots \quad 7.2$$

where $$\overline{i_D^2} = 2qI_{eq}B \quad \ldots\ldots\ldots\ldots\ldots\ldots\ldots\ldots\ldots\ldots \quad 7.3$$

$$\overline{i_G^2} = 2qI_GB \quad \ldots\ldots\ldots\ldots\ldots\ldots\ldots\ldots\ldots\ldots \quad 7.4$$

and $$\overline{i_{R_1}^2} = 2qI_{R_1}B \quad \ldots\ldots\ldots\ldots\ldots\ldots\ldots\ldots\ldots\ldots \quad 7.5$$

The expression for I_{R_1} is

$$I_{R_1} = \frac{2KT_1}{qR_1} \quad \ldots\ldots\ldots\ldots\ldots\ldots\ldots\ldots\ldots\ldots \quad 7.6$$

By substituting equations 7.3, 7.4, 7.5 and 7.6 into equation 7.2, it is found that

$$I_{eq} = I_G + \frac{2KT_1}{qR_1} \quad \text{..... 7.7}$$

The variables on the right hand side of the equal sign are all known and hence I_{eq} may be determined. The values for I_{eq} are shown plotted in figure 7.8.

Noise measurements at the peak and valley voltages

The noise measurements at the peak and valley voltages are performed in rather a unique manner since the impedance of the tunnel diode at these bias voltages is essentially infinite. The test procedure, being similar in nature to the procedure used for the positive conductance region, is as follows.

With the calibrating signal switched on and with a resistor R_1 connected across the terminals of X - X^1, a received output meter deflection M_s is obtained. The tunnel diode is now placed across the terminals X - X^1 in parallel with resistor R_1 and the tunnel diode bias is varied until the same deflection M_s is again obtained. For this tunnel diode bias the impedance across the resistor R_1 is the same as the impedance across the parallel arrangement of the tunnel diode and resistor R_g.

The calibrating signal is then switched off and with

Figure 7.8

Comparison of the theoretical and experimental noise present in the tunnel diode 1N2939.

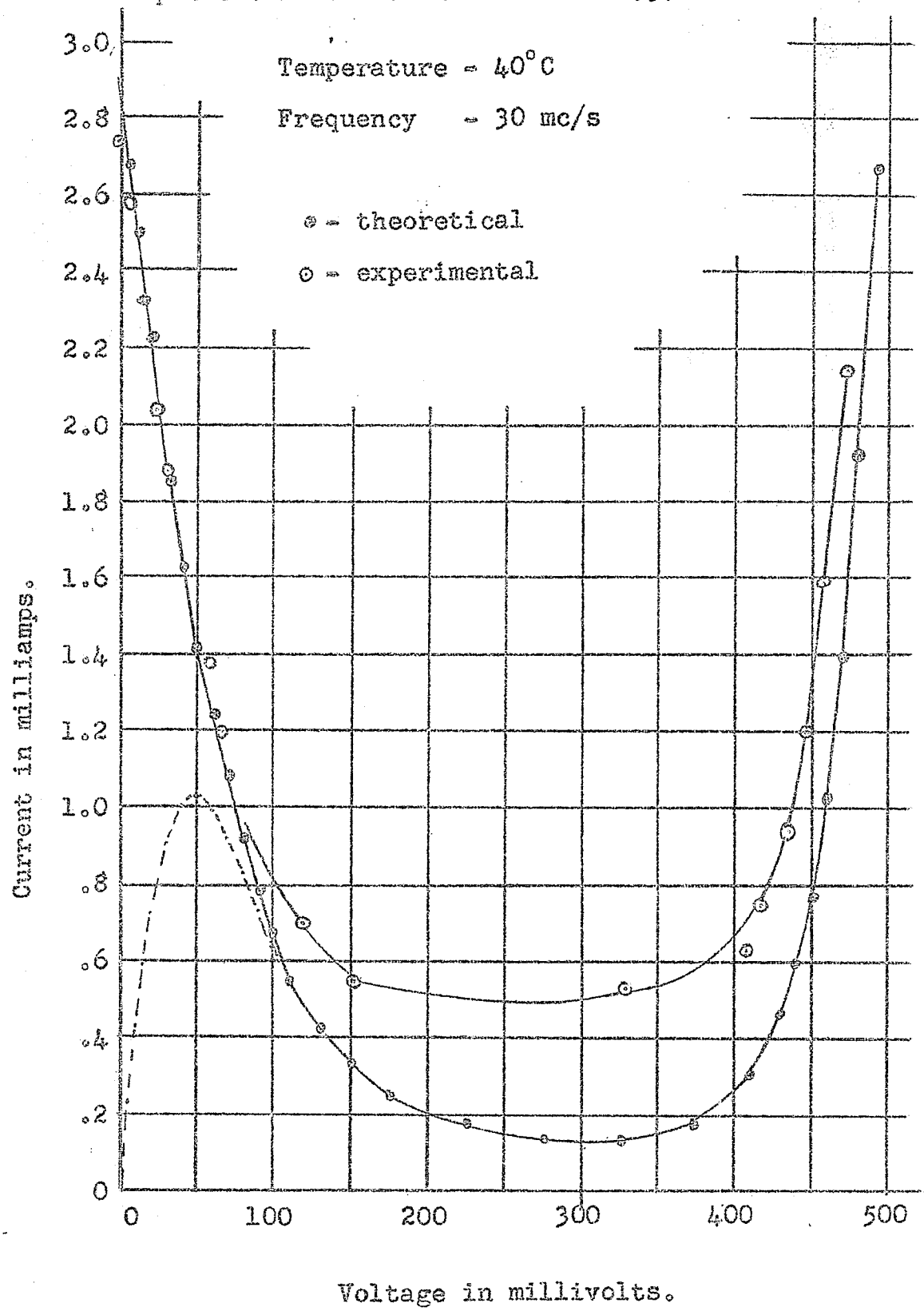

the tunnel diode and resistor connected across the terminals $X - X^1$ as shown in figure 7.9, a received output meter deflection M_D is obtained.

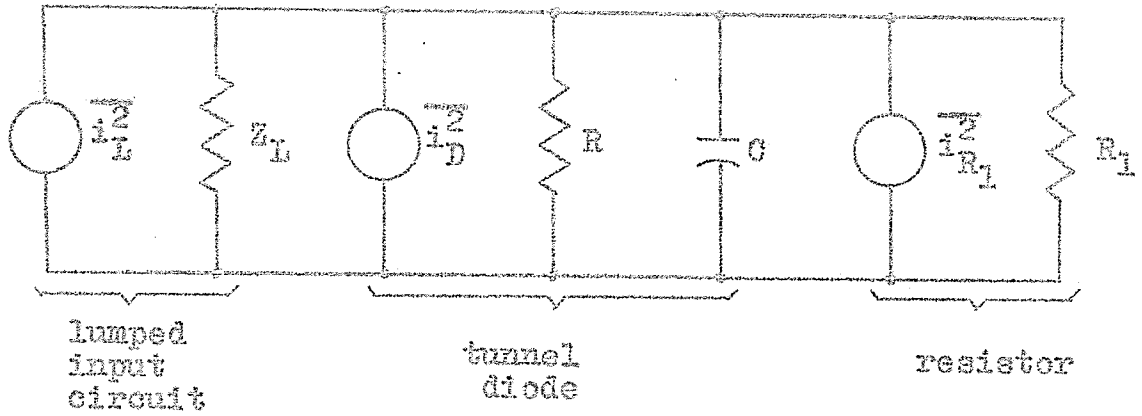

Figure 7.9 Schematic noise measurement diagram for the peak and valley voltages.

The tunnel diode is now removed and with only resistor R_1 connected across the terminals $X - X^1$ as shown in figure 7.6, the noise output of the noise generator is increased until the same deflection M_D is again obtained. The noise generated by the noise generator is now equal to the noise generated by the tunnel diode.

From figures 7.6 and 7.9

$$\overline{i_{R_1}^2} + \overline{i_L^2} + \overline{i_D^2} = \overline{i_G^2} + \overline{i_{R_1}^2} + \overline{i_L^2} \quad \text{..... 7.8}$$

and it therefore follows that

$$I_{eq} = I_G \quad \text{..... 7.9}$$

Noise measurement in the negative conductance region

Noise measurement in the negative conductance region is similar to the noise measurement at the peak and valley voltages except that the resistance R_1 in figure 7.9 is replaced by resistance R_2. For a particular tunnel diode bias in the negative conductance region, the impedence across the parallel arrangement of the tunnel diode and resistor R_2 is made equal to the impedance across the resistor R_1.

From figures 7.6 and 7.9

$$\overline{i_L^2} + \overline{i_{R_2}^2} + \overline{i_D^2} = \overline{i_L^2} + \overline{i_{R_1}^2} + \overline{i_G^2} \quad \ldots\ldots\ldots\ldots\ldots\ldots \quad 7.10$$

and the equivalent noise current I_{eq} of the tunnel diode is determined as

$$I_{eq} = I_G + \frac{2KT_1}{qR_1} - \frac{2KT_2}{qR_2} \quad \ldots\ldots\ldots\ldots\ldots\ldots \quad 7.11$$

where $T_1 = T_2 = 313^{\circ}$ Kelvin.

II. NOISE MEASUREMENTS AT 60 MEGACYCLES PER SECOND

In order to determine whether a frequency dependent noise was present at 30 megacycles per second it was necessary to perform noise measurements at an increased frequency. Since a 55-210 megacycles per second broadband amplifier was available, a frequency of 60 megacycles per second was found

convenient. The procedure used for noise measurements at this frequency was identical to the procedure used at 30 megacycles per second. The noise generated by the tunnel diode was measured at a temperature of 50° centigrade.

The block and schematic diagrams are shown in figures 7.10 and 7.11 respectively. Photographs of the receiving system are shown in figures 7.13, 7.14 and 7.15. A 0.25 wavelength short circuited transmission line was used for supplying the tunnel diode bias. The capacitor C_4 in figure 7.11 serves as the short circuit to the transmission line. The low-pass filter, consisting of elements C_4, C_5 and L_3, prevents any external 60 megacycle signal from entering the input circuit.

Proper precautions must be taken when using a broadband amplifier for noise measurements. One rejection filter at 120 megacycles per second and another at 150 megacycles per second were required at the output of the amplifier. Each consisted of a one-half wavelength short-circuited transmission line at its respective frequency. It was assumed that the filters attenuated the 60 megacycle per second signal by a negligible amount. The 120 megacycle per second filter prevents any 120 megacycles per second noise at the output of the amplifier from mixing with the local oscillator signal of 90 megacycles per second. The other filter prevents any 150 megacycles per second noise at the output of the amplifier from mixing with the second harmonic of the local oscillator signal. Both filters were tuned to their respective frequencies by applying appropriate signals to the input of the amplifier.

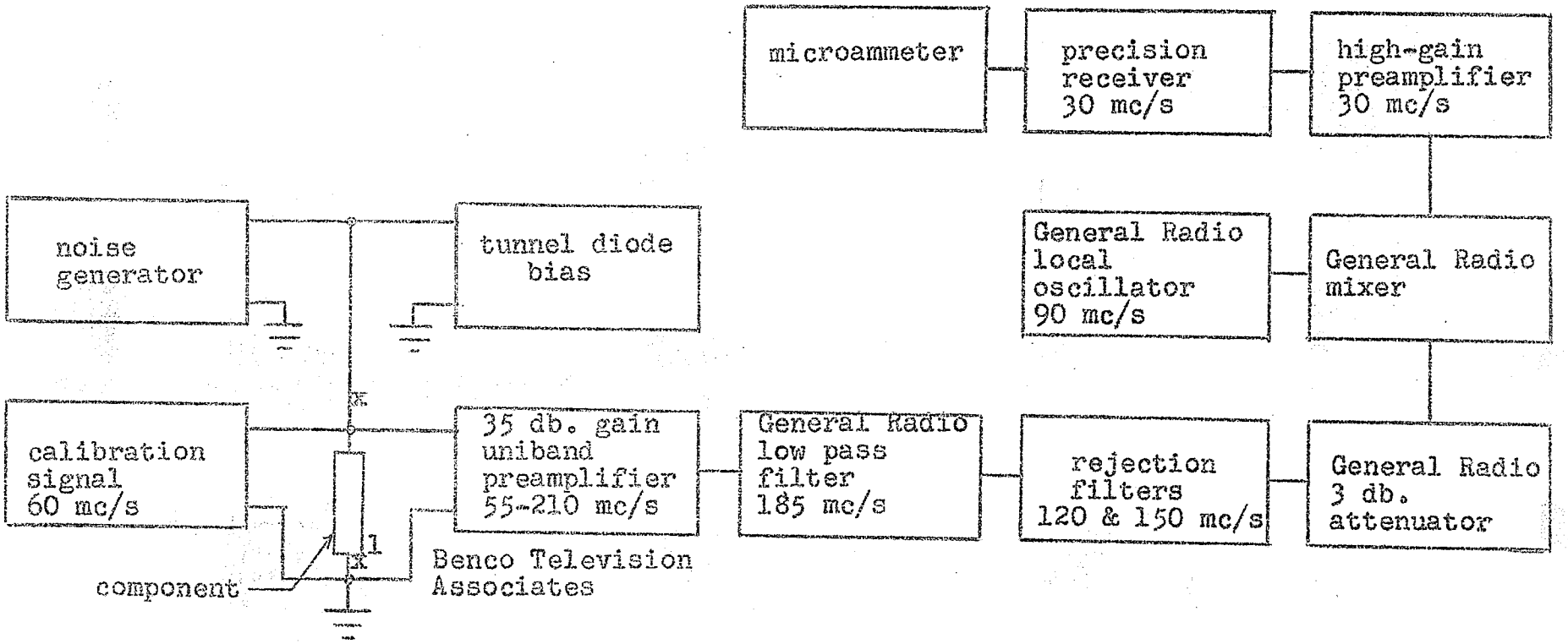

Figure 7.10

Block diagram of noise measurement circuit at 60 megacycles per second.

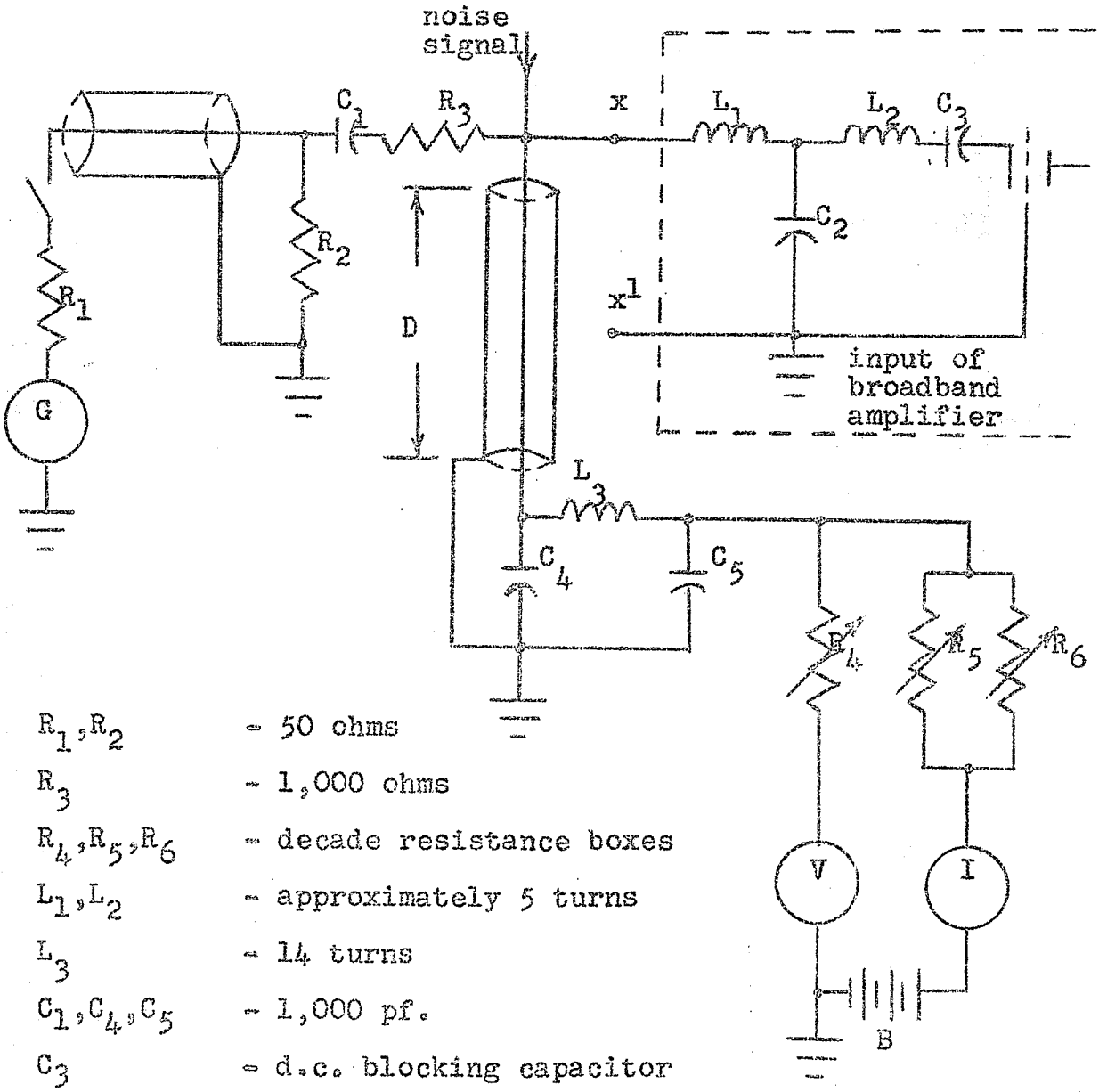

R_1, R_2	- 50 ohms
R_3	- 1,000 ohms
R_4, R_5, R_6	- decade resistance boxes
L_1, L_2	- approximately 5 turns
L_3	- 14 turns
C_1, C_4, C_5	- 1,000 pf.
C_3	- d.c. blocking capacitor
V	- microammeter
I	- milliammeter
G	60 mc/s signal generator
D	- 125 cm. or 0.25 wavelength at 60 mc/s

Figure 7.11

Schematic diagram of noise measurement circuit at 60 megacycles per second.

Figure 7.12

Comparison of the theoretical and experimental noise present in the tunnel diode 1N2939.

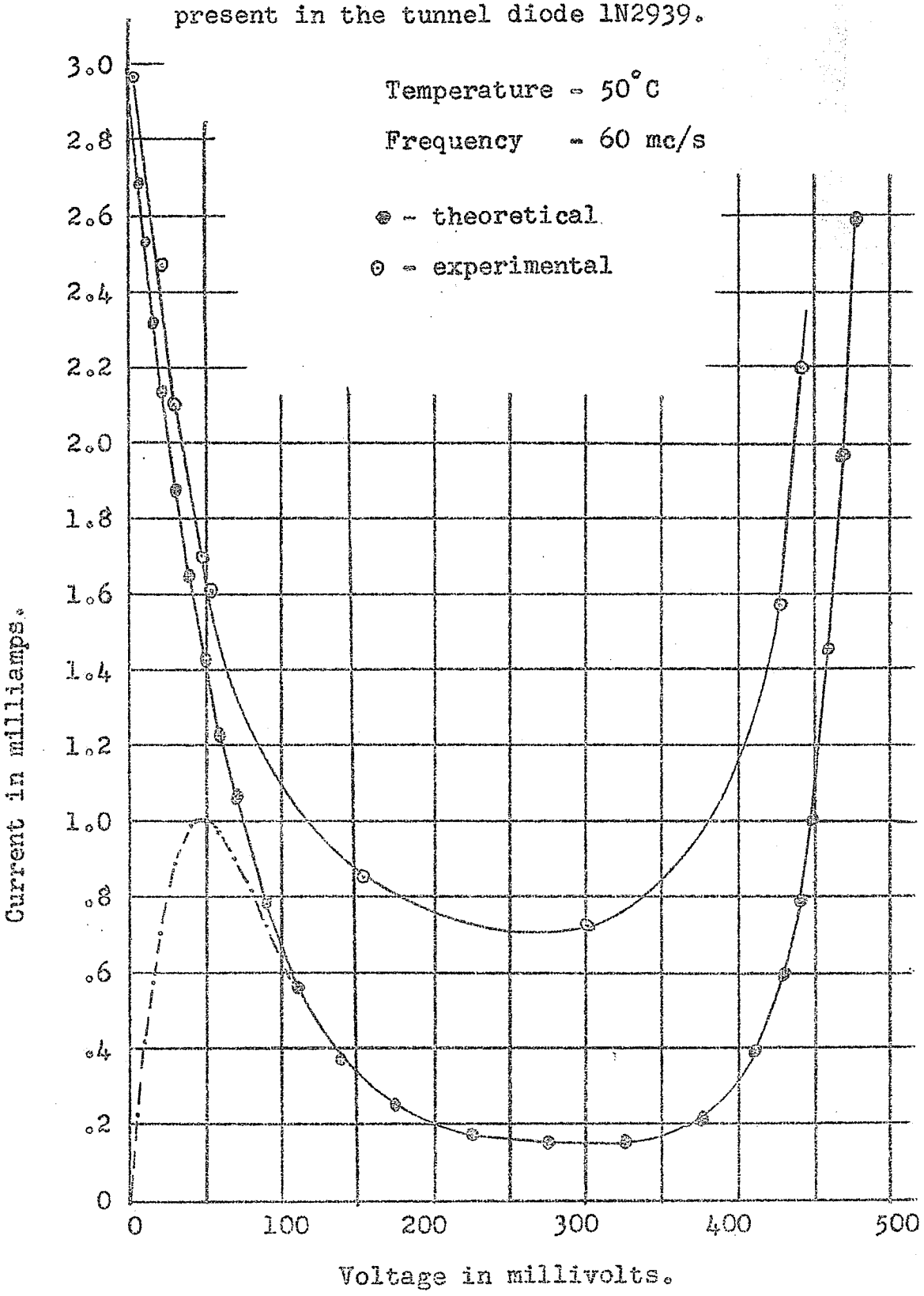

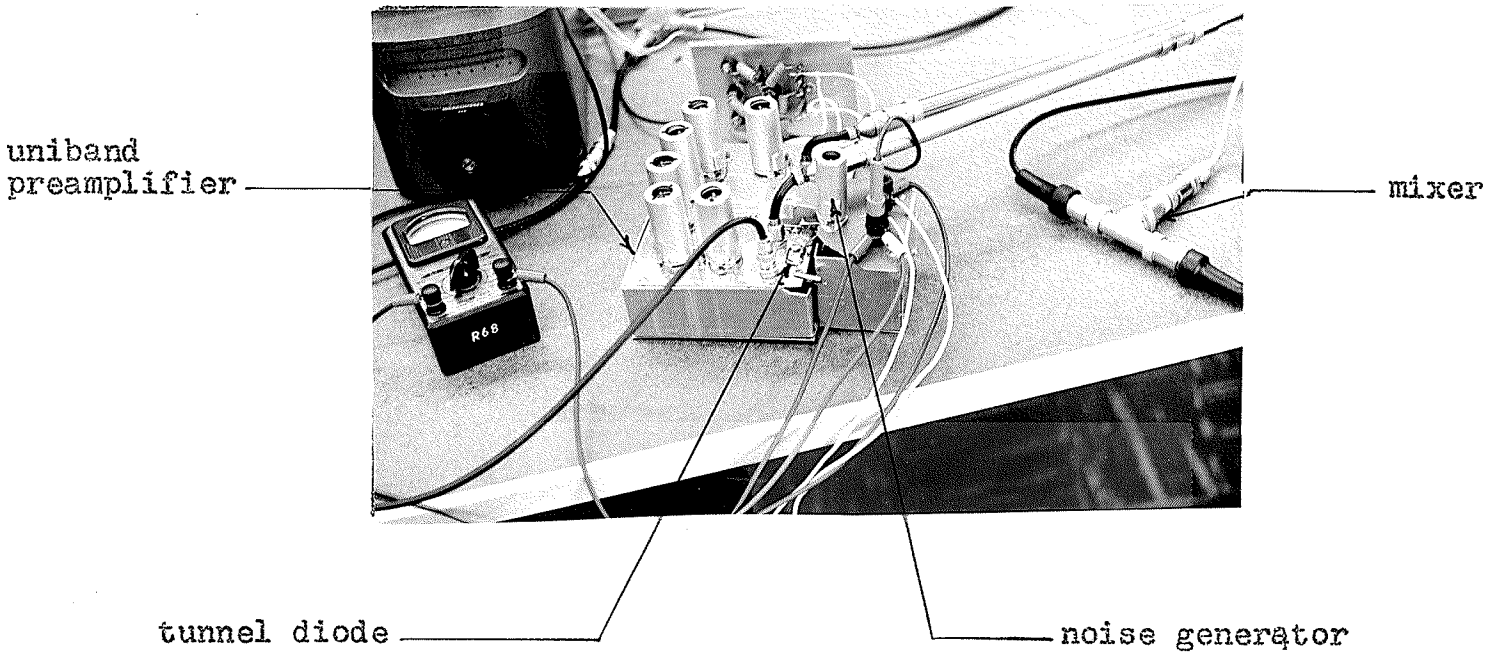

Figure 7.13

Input system of the 60 megacycles per second receiving system.

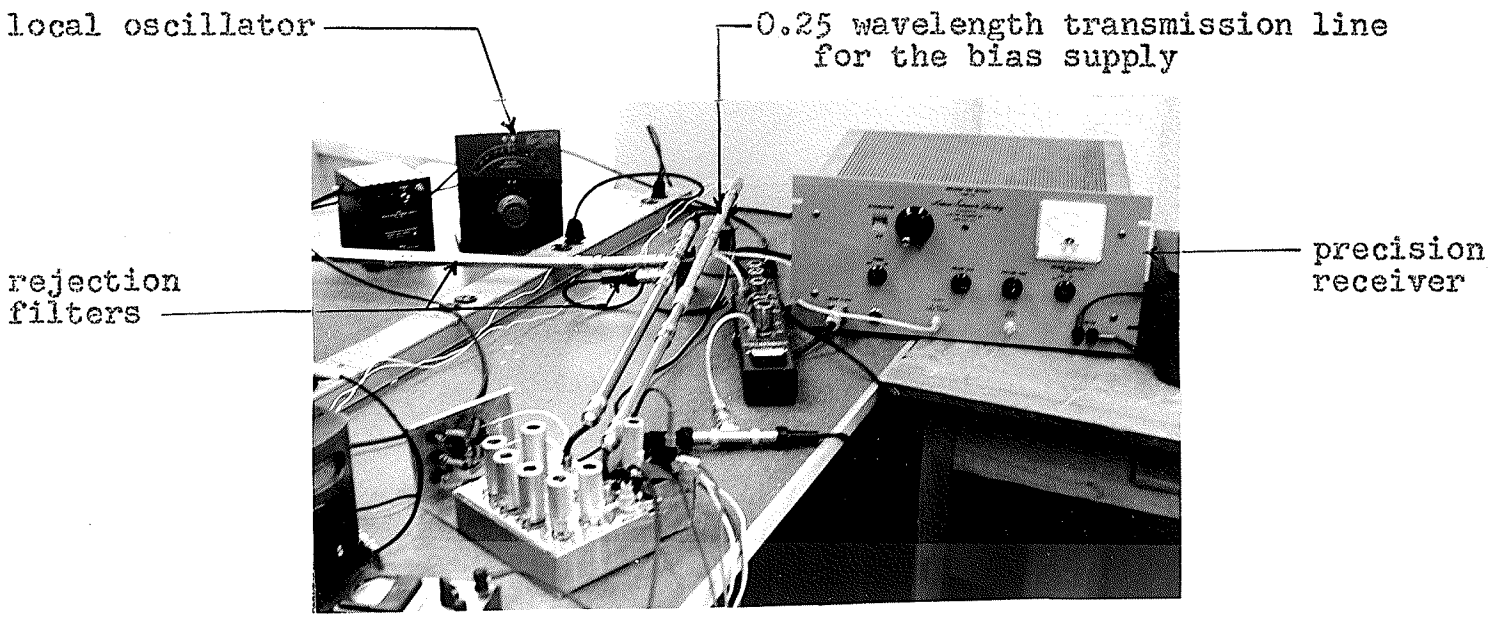

Figure 7.14

The 60 megacycles per second receiving system showing the transmission line filters.

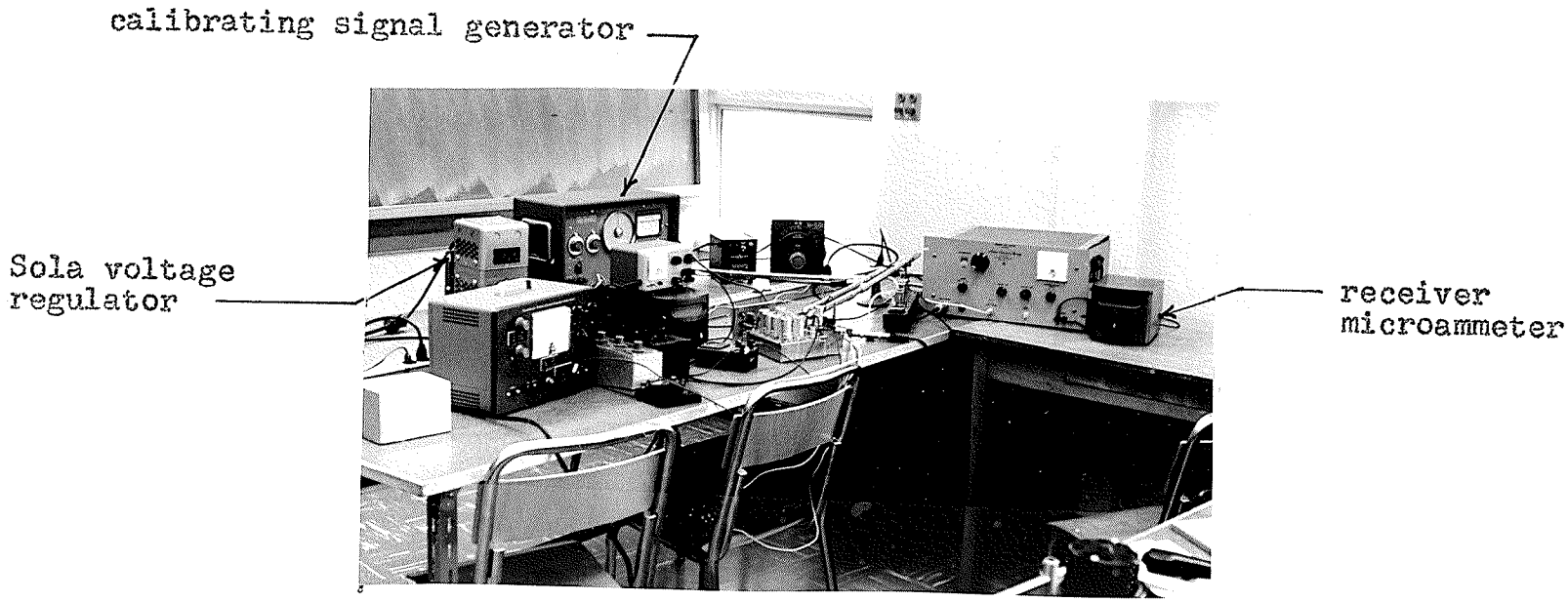

Figure 7.15

The complete 60 megacycles per second receiving system.

CHAPTER VIII

DISCUSSIONS AND CONCLUSIONS

I. DISCUSSIONS

Figure 7.8 shows the comparison of the theoretical and experimental equivalent noise current present in the tunnel diode 1N2939 at a frequency of 30 megacycles per second. In the low bias region the curves for the experimental and theoretical noise almost coincide but in the valley region the experimental noise is substantially greater than the theoretical noise. This implies that either the excess current I_x produces more noise than shot noise or that a reverse tunneling current I'_x is present in this region. The calculated I'_x, which is based on the noise current in figure 7.8, is shown in figure 2.8. It is assumed that I'_x is uncorrelated with the current I_x. Agouridis and van Vliet considered that a reverse current I'_x is unlikely.[13] However, it is possible that the current I_x exhibits more than shot noise as mentioned by Tiemann.[4] The additional noise in the valley region is not considered to be frequency dependent since there is no indication that the noise decreases with frequency when comparing figures 7.8 and 7.12. At a large forward bias the theoretical and experimental noise currents appear to converge which indicates that the current I_f produces full shot noise only.

Figure 7.12 shows the theoretical and experimental noise curves at a frequency of 60 megacycles per second. The experimental noise current is greater than the theoretical for the complete forward bias range. Since the temperature at which the noise was measured is substantially greater than room temperature, a temperature error could be present due to the handling of the components. The general shape of the experimental noise curve is consistent with the experimental noise curve in figure 7.8.

The values of the parasitic resistance R_s and the capacitance C of the tunnel diode were not determined. The measurement of R_s involves the negative biasing of the tunnel diode to currents far exceeding the maximum current rating of the diode. An ample supply of diodes was not available and therefore no measurements were attempted. The capacitance C could not be measured since a low signal level bridge instrument was not available for the frequencies considered.

The bandwidth error is almost nonexistent except for a small effect due to the diode capacitance C. No error can be attributed to the nonlinear amplification of the system. The error due to the parasitic resistance is relatively large for zero bias. However no correction was made because of the difficulty in performing the calculations. If the calculations had been performed a number of approximations would have been necessary. The error due to the parasitic resistance is considered negligible in all regions except

for the zero bias and for the extreme end of the high bias region.

The peak current variations for varying temperatures as shown in figure A.2 correspond very closely to the peak current variation as shown on page 13, reference 22.

II. FURTHER APPLICATIONS

This thesis provides the groundwork for future component noise measurements. The noise measurement of a conventional diode would involve a direct application of the tests outlined in this thesis. To avoid temperature error due to the deviation of the temperature at the input of the amplifier from room temperature, a half wavelength transmission line could possibly be used at the input.

III. CONCLUSIONS

No decrease in the noise readings were noted at 60 megacycles per second. It can therefore be concluded that the frequency dependent noise or excess noise of the tunnel diode was absent at 30 megacycles per second.

From the graph in figure 7.8 it can be seen that the measured equivalent noise current in the low bias region is very nearly equal to the calculated equivalent noise current. On the basis of the previously mentioned theory that only the Esaki and Zener currents exist in the low bias region, it

can be concluded that the two currents are uncorrelated and exhibit full shot noise.

From the results obtained in figures 7.8 and 7.12 it can be concluded that a greater noise than full shot noise due to the current I_x is present in the valley region.

In the high bias region the measured noise tends to converge to the calculated noise. It can therefore be concluded that the high bias current I_f of the tunnel diode generates full shot noise.

APPENDICES

APPENDIX A

THE CURRENT-VOLTAGE MEASUREMENT

One of the important factors for performing noise calculations is that an accurate current-voltage characteristic of the tunnel diode may be established. Figure A.1 shows the circuit which is used for the measurement of the current-voltage characteristic. Measurements were made for temperatures varying up to 100° centigrade as shown in figure A.2. The temperature-controlled oven is shown in figure A.3.

The value of the resistor R_5 is known to four place accuracy at each temperature for which the current-voltage characteristic is measured. The product KR_4 is adjusted to equal R_5, where K is some arbitrary value, to obtain a suitable deflection on the microammeter.

The value of I_R is calculated as

$$I_R = KI_I \quad \text{..... A.1}$$

The tunnel diode current is calculated according to the expression

$$I_D = I_R + I_I - I_V \quad \text{..... A.2}$$

Substituting equation A.1

$$I_D = (1 + K)\, I_I - I_V \quad \text{..... A.3}$$

I_I and I_V are the meter readings on the microammeters.

The tunnel diode voltage V_D is obtained from the expression

$$V_D = R_3 I_V \quad \text{..... A.4}$$

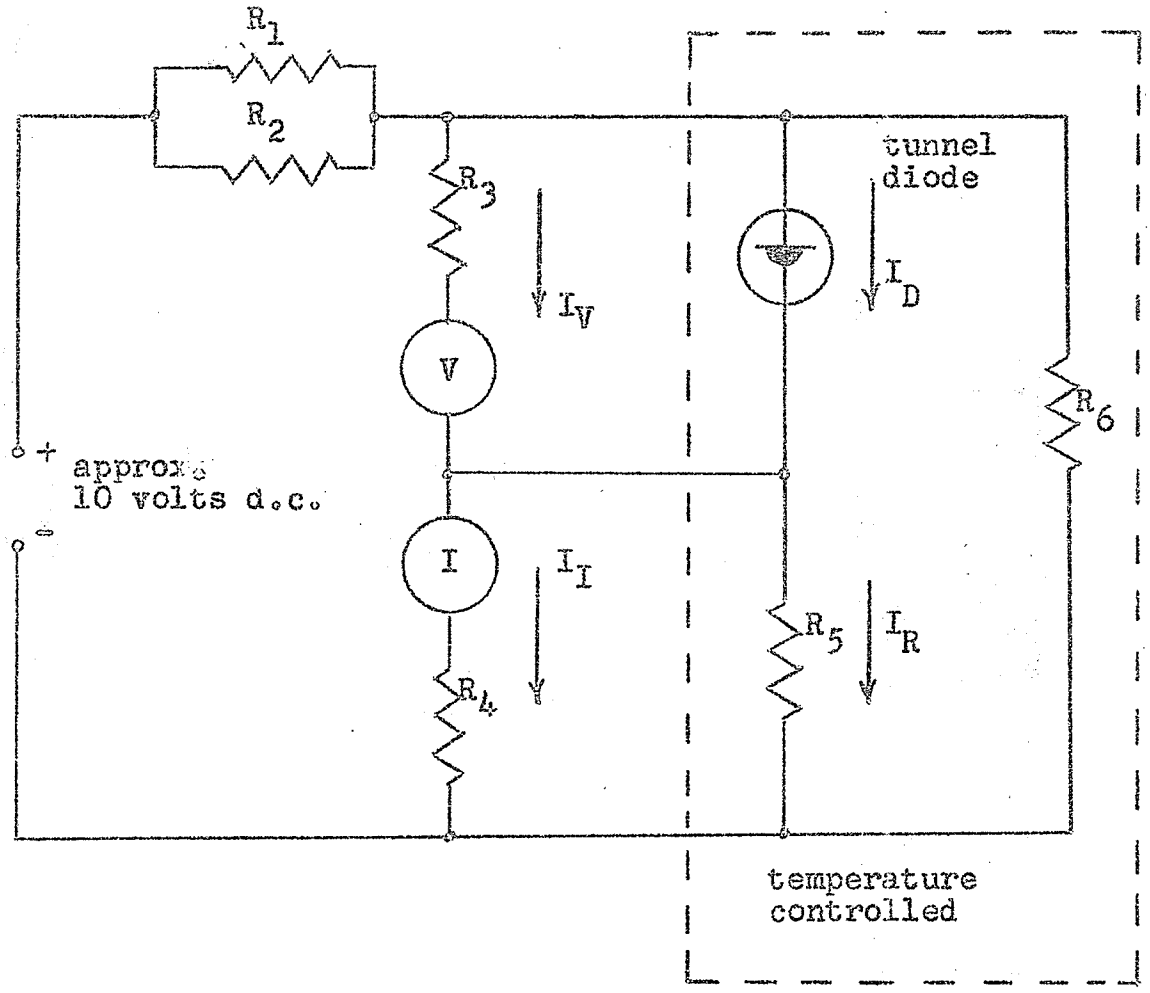

R_1, R_2 - decade resistance boxes

R_3, R_4 - decade resistance boxes (1%)

R_5 - 22.40 ohms at temperature of 30 C

R_6 - approximately 56 ohms

V, I - microammeters (3 ohms)

Figure A.1

Measurement circuit for the tunnel diode characteristic.

Figure A.2

Variation of the tunnel diode characteristic with temperature.

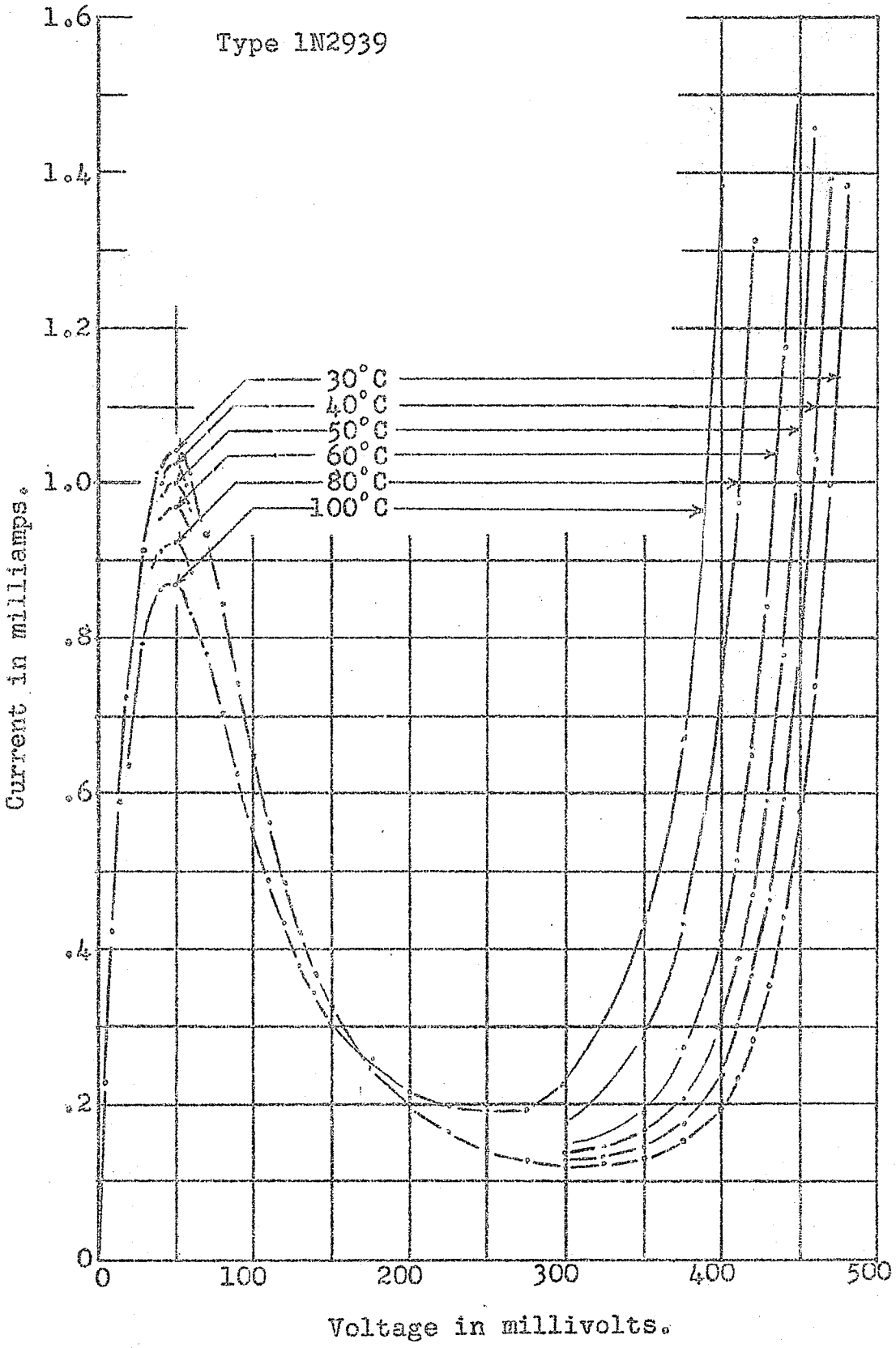

where R_3 is adjusted to obtain a suitable deflection on the meter V.

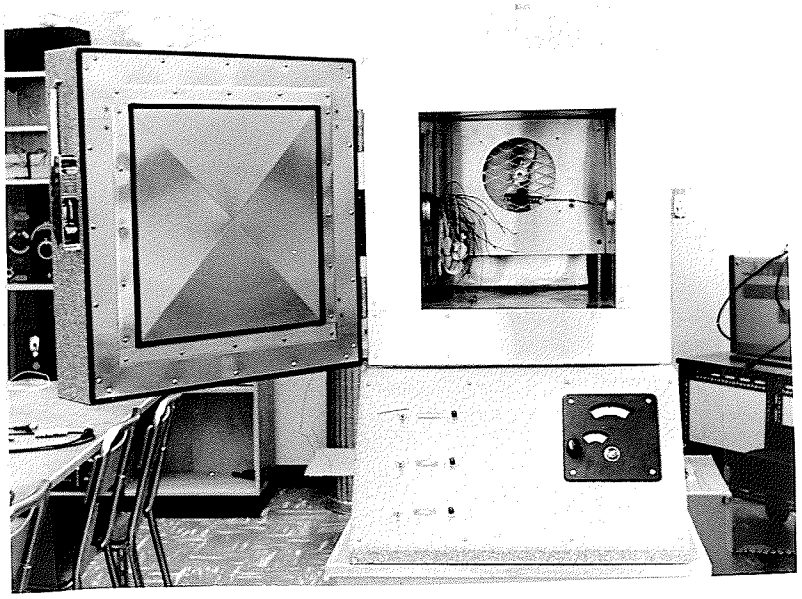

Figure A.3 Temperature-controlled oven

APPENDIX B

RECEIVER NOISE FIGURE

I. DEFINITION OF NOISE FIGURE

The sensitivity of a system used for electrical measurements is ultimately limited by the noise fluctuations inherent in the components of the system. In the case of a receiver, the inherent noise of the system is usually dependent upon the input stages because noise entering at these stages receives the greatest amplification. Noise in receivers includes fluctuation noise, microphonics, and stray pick-up in leads. Fluctuation noise, examples of which have been mentioned earlier, appears inevitable in all electronic circuits.

The measure of noise generated within the receiver circuits is known as the noise figure. It is defined as the available signal to noise power ratio at the input divided by the signal to noise power ratio at the output. The noise figure is expressed as

$$F = \frac{S_i/N_i}{S_o/N_o} \quad \text{..... B.1}$$

where S_i is the input signal power; N_i is the input noise power; S_o is the output signal power; N_o is the output noise power.

II. MEASUREMENT OF RECEIVER NOISE FIGURE

The procedure used for determining the noise figure is identical for the 30 and 60 megacycles per second receiving systems. Only the 30 megacycle per second receiving system is outlined.

For the noise figure measurements the resistor R_1 of the noise generator in figure 7.3 and the resistors R_2 and R_3 as shown in figure 7.2 will be considered as parts of the receiving system. Any noise generated by them will therefore be included in the noise figure.

Consider the block diagram of figure 7.1. The noise generator and calibration signal are switched off. A resistor R_1 is placed across the terminals $x - x^1$. With the high-gain preamplifier set on almost maximum gain an output meter deflection M_1 is obtained. The precision receiver consists of a precision attenuator followed by a post amplifier. It is considered that the post amplifier contributes very little noise, if any, to the noise of the complete receiver system since the signal level at the input of the post amplifier is large. An attenuation of 3 decibels is added by the precision attenuator. The filament voltage of the noise generator is increased from zero to a value which will give an output meter deflection of M_1. The average diode current I_G is then noted.

The ratio of the mean square currents is also the ratio

of the powers.

Hence $$\frac{S_i}{N_i} = \frac{i_G^2}{\overline{i^2}} R_1 \quad \text{..... B.2}$$

From equations 7.4 and 7.5

$$\frac{S_i}{N_i} = \frac{q\, I_G R_1}{2\, KF_1} \quad \text{..... B.3}$$

The output noise was doubled and therefore

$$S_o = N_o \quad \text{..... B.4}$$

The noise figure is then

$$F = \frac{q}{2KF_1} I_G R_1 \quad \text{..... B.5}$$

All the values on the right hand side of the equal sign are known and the noise figure F is shown plotted for various values of R in figure B.1.

Figure 8.1

Noise figure measurements.

Receiver system

△ - 60 mc/s

o - 30 mc/s

Temperature

△ - 50°C

o - 40°C

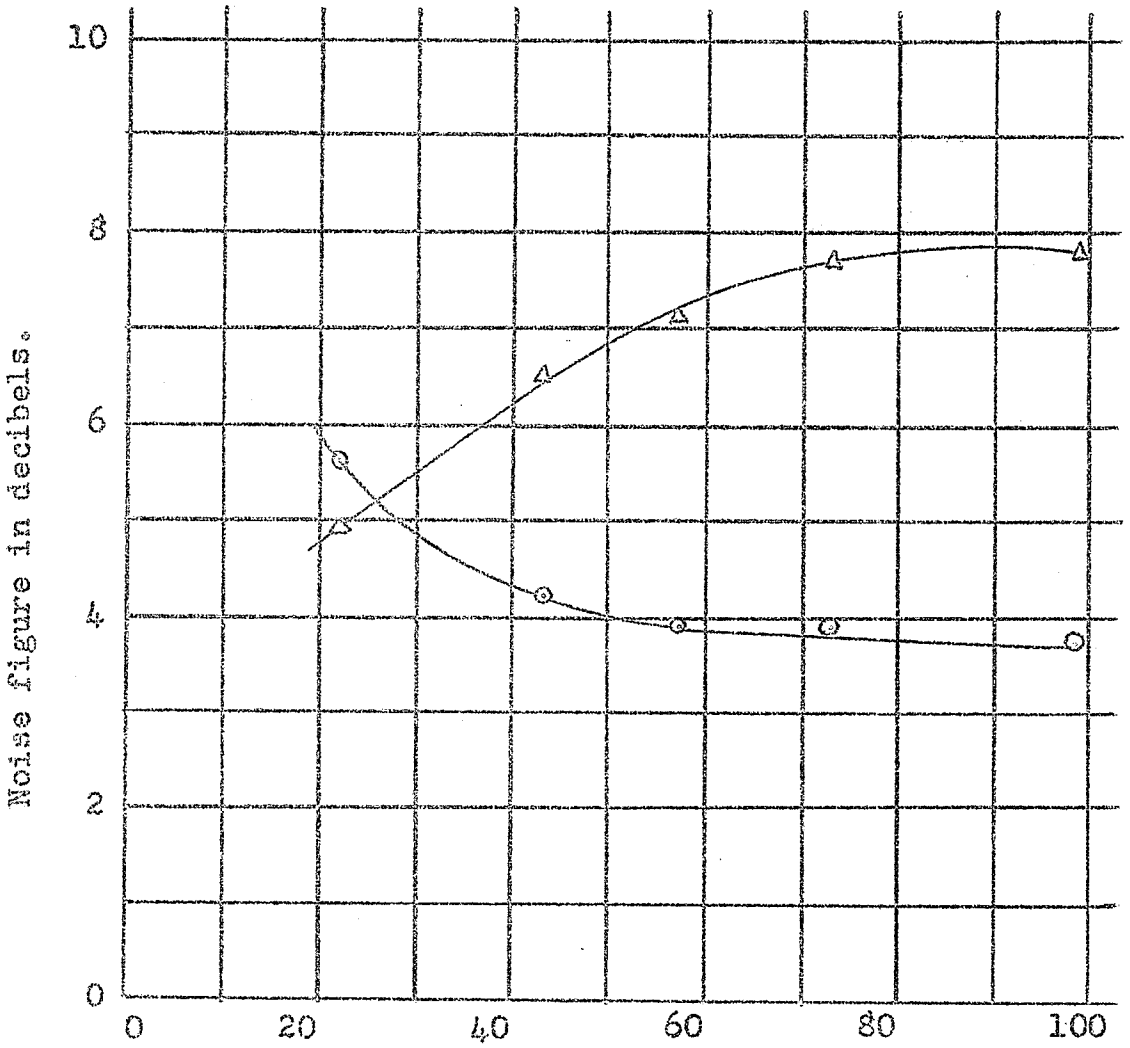

APPENDIX C

SPECIFICATIONS OF THE TUNNEL DIODE 1N2939

Many of the electrical characteristics were not obtained by experiment and therefore a list of the specifications for a typical tunnel diode 1N2939 is justified.

ABSOLUTE MAXIMUM RATINGS

Forward Current (-55 to +100°C)	5 ma
Reverse Current (-55 to +100°C)	10 ma
Storage Temperature	- 55 to +100°C
Operating Junction Temperature	- 55 to +100°C
Lead Temperature, 1/16" ± 1/32" From case for 10 seconds	260°C

ELECTRICAL CHARACTERISTICS (25°C) (1/8" Leads)

	Typical Value	
Peak Point Current	1.0	ma
Valley Point Current	0.10	ma
Peak Point Voltage	70	mv
Valley Point Voltage	350	mv
Negative Conductance	6.6×10^{-3}	mho
Total Capacity	5.0	pf
Series Inductance	6×10^{-9}	henry
Series Resistance	1.5	ohm
Resistive Cutoff Frequency	2.2	Kmc/s
Self-resonant Frequency	.950	Kmc/s

BIBLIOGRAPHY

BIBLIOGRAPHY

1. Leo Esaki. New Phenomenon in Narrow Germanium P-N Junctions. Physical Review, Vol. 109, p.603; Jan. - March, 1958.

2. P. Aigrain. Theory of Impurity Bands with Randomly Distributed Centres. Physica, Vol. 20, p.978; 1954.

3. R.R.N. Chang. Low Noise Tunnel Diode Amplifier. Proc. IRE, Vol. 47, p.1268; July 1959.

4. J.J. Tiemann. Shot Noise in Tunnel Diode Amplifiers. Proc. IRE, Vol. 48, p.1418; Aug. 1960.

5. B. Sklar. The Tunnel Diode - Its Action and Properties. Electronics, Vol.32, p.55; Nov.6, 1959.

6. Tunnel Diode - New Electronic Work Horse. Electronic Industries, Vol. 18, p.82; August 1959.

7. F.H. Mitchell. Deriving the Tunnel Diode Curve. Electronic Industries, Vol. 20, p.96; Oct. 1961.

8. R.A. Pucel. The Equivalent Noise Current of Esaki Diodes. Proc. IRE, Vol. 49, p.1080; June, 1961.

9. A.G. Chynoweth, W.L. Feldmann, R.A. Logan. Excess Tunnel Current in Silicon Esaki Junctions. Physical Review, Vol.121, No.3, p.684; Feb. 1961.

10. C.J. Christenson, G.L. Pearson. Spontaneous Resistance Fluctuations in Carbon Microphones and Other Granular Resistances. Bell System Tech. J., Vol.15, p.197; 1936.

11. R. La Rosa, C.R. Wilhelmsen. Theoretical Justification for Shot Noise Smoothing in the Esaki Diode. Proc. IRE, Vol.48, p.1418; Aug.,1960.

12. C.A. Lee, A. Yariv. Comment on Shot-Noise Smoothing Mechanism Proposed by La Rosa and Wilhelmsen. Proc. IRE, Vol. 49, p.1695; Nov.,1961.

13. D.C. Agouridis, K.M. van Vliet. Noise Measurements on Tunnel Diodes. Proc. IRE, Vol.50, p.2121; Oct., 1962.

14. J.B. Johnson. Thermal Agitation of Electricity in Conductors. Physical Review, Vol. 32, p.97; 1928.

15. H. Nyquist. Thermal Agitation of Electrical Charge in Conductors. Physical Review, Vol.32, p.110; 1928.

16. R.H. Mattson, A. van der Ziel. Shot Noise in Germanium Filaments. Journal of Applied Physics, Vol.24, p.222; 1953.

17. C.N. Berglund. Measurement of Shot Noise in Tunnel Diodes at Low Forward Voltages. Unclassified document, Massachusetts Institute of Technology, Aug.,1961.

18. J.L. Bower, P.M. Schultheis. Introduction to the Design of Servomechanism. John Wiley and Sons. Chapter 4;1958.

19. G. Wade. Low-Noise Amplifiers for Centimeter and Shorter Wavelengths. Proc. IRE, Vol.49, p.887; May, 1961.

20. H. Boyet, D. Fleri, C.A. Renton. Stability Criteria for a Tunnel Diode Amplifier. Proc.IRE, Vol.49, p.1937; Dec.,1961.

21. A van der Ziel. Noise. Prentice-Hall, 1954.
(a) p.196; (b) p.9; (c) p.213; (d) p.208; (e) p.65.

22. General Electric. Tunnel Diode Manual. First edition, 1961.

23. G.E. Valley, H. Wallman. Vacuum Tube Amplifiers. McGraw-Hill, p.169; 1948.

24. A.W. Lo, R.O. Endres, J. Zawels, F.D. Waldhauer, C.C. Cheng. Transistors Electronics. Prentice-Hall, p.20; 1955.

25. F.N.H. Robinson. Noise in Electrical Circuits. Oxford University Press. 1962. (a) p.46.

26. M. Schwartz. Information Transmission, Modulation, and Noise. McGraw-Hill, 1959. (a) p.225.

27. E.P. Tilton. Noise Generators-Their Uses and Limitations. QST, p.10; July,1953.

28. E.L. Bonin, J.R. Biard. Tunnel-Diode Series Resistance. Proc. IRE, Vol.49, p.1679; Nov.1961.

29. A. Yariv, J.S. Cook. A Noise Investigation of Tunnel Diode Microwave Amplifiers. Proc. IRE, p.739; April 1961.

30. C.N. Berglund. An Experimental Investigation of Noise in Tunnel Diodes. Unclassified document, Massachusetts Institute of Technology, July, 1961.